Title

Adaptation to low parasite abundance affects immune investment strategy and immunopathological responses of cavefish

Authors

Robert Peuß[1], Andrew C. Box[1], Shiyuan Chen[1], Yongfu Wang[1], Dai Tsuchiya[1], Jenna L. Persons[1], Alexander Kenzior[1], Ernesto Maldonado[2], Jaya Krishnan[1], Jörn P. Scharsack[3,4], Brian P. Slaughter[1] & Nicolas Rohner[1,5]

Author for correspondence:

Nicolas Rohner (nro@stowers.org)

Affiliation

[1]Stowers Institute for Medical Research, Kansas City, MO, USA

[2]EvoDevo Research Group, Unidad Académica de Sistemas Arrecifales, Instituto de Ciencias del Mar y Limnología, Universidad Nacional Autónoma de México, Puerto Morelos, Quintana Roo, Mexico

[3]Institute for Evolution and Biodiversity, University of Münster, Münster, Germany

[4]present address: Thünen Institute of Fisheries Ecology, Bremerhaven, Germany

[5]Department of Molecular & Integrative Physiology, University of Kansas Medical Center, Kansas City, KS, USA

Abstract

Reduced parasite infection rates in the developed world are suspected to underlie the rising prevalence of autoimmune disorders. However, the long-term evolutionary consequences of decreased parasite exposure on an immune system are not well understood. We used the Mexican tetra *Astyanax mexicanus* to understand how loss of parasite diversity influences the evolutionary trajectory of the vertebrate immune system by comparing river with cave morphotypes. Here, we present field data that affirms a strong reduction in parasite diversity in the cave ecosystem and show that cavefish immune cells display a more sensitive proinflammatory response towards bacterial endotoxins. Surprisingly, other innate cellular immune responses, such as phagocytosis, are drastically decreased in cavefish. Using two independent single-cell approaches, we identified a shift in the overall immune cell composition in cavefish as the underlying cellular mechanism, indicating strong differences in the immune investment strategy. While surface fish invest evenly into the innate and adaptive immune system, cavefish shifted immune investment to the adaptive immune system, and here, mainly towards specific T-cell populations that promote homeostasis. Additionally, inflammatory responses and immunopathological phenotypes in visceral adipose tissue are drastically reduced in cavefish. Our data indicate that long term adaptation to low parasite diversity coincides with a more sensitive immune system in cavefish, which is accompanied by a reduction of the immune cells that play a role in mediating the proinflammatory response.

44 Main text

45 Important efforts in hygiene and medical treatment in most industrialized countries have reduced
46 microbial and parasitic infections considerably[1]. While this indisputably improves health and
47 increases life expectancy, the diverse effects on the immune system are not well understood.
48 Host-parasite interactions are the major driving force in the evolution of the immune system[2].
49 From an evolutionary perspective, the maintenance and control of the immune system is
50 associated with costs[2,3], so a reduction in parasite diversity should theoretically increase the
51 fitness of the host.

52 Interestingly, the opposite has been observed. Based on a number of studies, it has been
53 hypothesized that decreased exposure to parasites or biodiversity in general has contributed to
54 the rising numbers of autoimmune diseases in the developed world[4-7]. This phenomenon has
55 been described as the "Old Friends hypothesis"[8], which argues that the reactivity of the vertebrate
56 immune system depends on the exposure to macroparasites (e.g., helminths) and microparasites
57 (e.g., bacteria, fungi and viruses). These parasites, that the host has coevolved with, are
58 necessary for the host to develop a proper functional immune system and to minimize
59 autoimmune reactions that potentially result in immunopathology (e.g. type 1 diabetes or
60 artheriosclerosis)[8].

61 Despite important insights into the physiological underpinnings of autoimmune diseases [9], we still
62 lack fundamental knowledge of how autoimmune diseases initially develop. Human populations
63 have only been confronted with this decreased parasite diversity for a couple of generations -
64 very recently in evolutionary terms. This raises the question of how the immune system adapts to
65 such environmental changes in the long term. Given the significant impact on fitness of
66 autoimmune disorders[9], evolutionary adaptations of the immune system to environments with low
67 biodiversity and thereby low parasite diversity[10,11] are likely to have been deployed.

68 The vertebrate immune system is composed of two main systems, the innate and the adaptive
69 immune system. The innate immune system is essential for the initial response against
70 pathogens. Given the short lifetime and high complexity, innate immune cells, such as
71 granulocytes, are thought to be very costly for the host[12]. The adaptive immune system of
72 vertebrates is defined by its long-term protection against pathogens (e.g. through the production
73 of pathogen-specific antibodies). Cells of the adaptive immune systems, such as B- and T-cells,
74 are thought to be less costly for the host due to their low complexity and longevity[12].

75 Given the differences in costs, it has been suggested that the vertebrate immune system is
76 capable of adjusting its immune investment strategy[13-15]. The host can invest to different degrees
77 into the innate or adaptive immune cells depending on the parasite abundance in the host
78 environment[13-15]. Accordingly, these different immune investment strategies result in specifc
79 differences in the immune responses[16].

80 Based on these phenotypic responses, adaption to environments with low parasite abundance
81 should result in a fixed immune investment strategy that is optimized for host fitness. To explore
82 this idea, we utilized an eco-immunological approach in the Mexican tetra *Astyanax mexicanus*,
83 to study how local adaptation of one host species to environments with a stark difference in
84 parasite diversity affects the immune system of the host.

85 There are cave and surface adapted populations of this species that have adapted to their
86 respective environments for approximately 50-200 thousand years[17,18]. One important hallmark
87 of cave environments is an overall decrease in biodiversity, including parasite diversity[19,20]. Here
88 we present field data from a cavefish population (Pachón) and one surface fish population (Río
89 Choy), which confirms a stark difference in macroparasite abundance between these two habitats
90 and indicates a higher immune activity of surface fish compared to cavefish under natural
91 conditions. Both, cavefish and surface fish populations can be bred and raised for generations in
92 the lab under identical environmental conditions, which readily facilitates the identification of

93 heritable changes. Therefore, we used lab populations that were derived from the wildtype
94 Pachón and Río Choy populations and an additional cavefish population (Tinaja) to investigate
95 immunological consequences deriving from adaptational processes to environments with low
96 parasite diversity. We demonstrate that cavefish immune cells display a more sensitive and
97 prolonged immune response of proinflammatory cytokines towards bacterial endotoxins *in vitro,*
98 similar to other vertebrate host species in environments with low biodiversity[21,22]. Using an image-
99 based immune cell clustering approach (Image3C) and single cell RNA sequencing (scRNAseq)
100 we show that the observed differences in the cellular immune responses are accompanied by
101 differences in the immune investment strategy, where cavefish produce more lymphoid cells
102 (adaptive immunity) than myeloid cells (innate immunity). We demonstrate that the altered
103 immune investment strategy does not generally affect all lymphocytes but mainly leads to an
104 overrepresentation of T-cells in cavefish.

105 Notably, we found that a large proportion of overrepresented T-cells in cavefish is represented by
106 *γδ*T-cells. This T-cell population is known for its regulatory role in several autoimmune diseases[23]
107 and the ability to recognize foreign antigens in a MHC (major histocompatibility complex)-
108 independent manner, thereby bridging the gap between the innate and adaptive immune
109 system[24]. Further scRNAseq analysis of the acute inflammatory response in fish treated with
110 lipopolysaccharides (LPS) revealed transcriptional changes in innate and adaptive immune cells
111 as well as in hematopoietic stem cells (HSCs) that may drive the observed changes in the immune
112 investment strategy. In addition, we observed differences in the adaptive response of T- and B-
113 cells, where cavefish display a higher activation response than surface fish. Finally, we show that
114 the reduction of granulocytic and monocytic cells in cavefish leads to reduced immunopathological
115 consequences for visceral fat storage, which has been described as an adaptional response
116 towards low food supply in the cave environment[25,26].

117 We started our investigation by collecting wild fish in their natural habitat to study the differences
118 in parasite abundance between river and cave environments. The differences in parasite
119 abundance between river and cave habitats of *A. mexicanus* have not been studied in detail and
120 are mainly based on assumptions that derive from theoretical models[10]. We collected 16 surface
121 fish (Río Choy) and 16 cavefish (Pachón), respectively (Fig. 1a), and examined them for parasite
122 infections as described before[27]. We found varying numbers of endo- and ectoparasites in surface
123 fish (Fig. 1b, see also Figure S1). Interestingly, we did not detect macroparasite infections in the
124 sampled cavefish (Fig. 1b). While we cannot exclude the possibility of viral or bacterial infections
125 in the cavefish population, we did not detect any obvious signs of systemic or tissue specific
126 infections during the parasitological examination. The lower parasite infection rate in wild cavefish
127 is also reflected in a significant lower spleen somatic index (an elevated immune activity in fish
128 coincides with a swelling of the spleen and increases spleen somatic index[28]) in wild cavefish
129 compared to the surface fish samples (Fig. 1c; mean spleen somatic index in surface fish of 0.663
130 vs. mean spleen somatic index in cavefish of 0.304; p = 0.0047, One-way ANOVA). Given the
131 strong impact of host – parasite interaction on the evolution of the immune system[2], we speculated
132 that these extreme differences in parasite abundance between cavefish and surface fish
133 environment result in functional and/ or physiological changes to the cavefish immune system.

134 To explore immunological differences in the potential to develop immunopathological phenotypes
135 between surface fish and cavefish, we first investigated the proinflammatory immune response,
136 which generally precedes immunopathological phenotypes[29]. To trigger such a proinflammatory
137 response we used bacterial endotoxins, LPS, in cultures with extracted leukocytes. We focused
138 on the the pronephros (head kidney, HK) (Figure 1d), the main hematopoietic and lymphoid organ,
139 and a site of antigen representation in teleost fish [30]. We incubated head kidney cells from surface,
140 Pachón and Tinaja fish with LPS (20 µg/mL) for 1, 3, 6, 12 and 24 hours, respectively and
141 measured gene expression of the proinflammatory cytokines *il-1β*, *tnf-α*, *il-6 and g-csf* in relation

142 to control samples (saline (PBS)) using RT-qPCR (Figure 1e, see Table S1 for details). Head
143 kidney cells from cavefish populations showed an overall greater inducible response upon LPS
144 treatment than head kidney cells from surface fish *in vitro* over time (Fig. 1e). Specifically, only
145 the gene expression of *il-1β* remained significantly elevated in surface fish after 24 hours (Figure
146 1e). In contrast, cavefish expression of all tested proinflammatory cytokines remained significantly
147 upregulated after 24 hrs. Since the cavefish response was saturated at this LPS concentration,
148 we repeated the analysis with a 100x fold lower LPS exposure (Fig. 1f). Here, LPS treated head
149 kidney cells from surface fish no longer displayed a significant response of any of the
150 proinflammatory cytokines, while Pachón cavefish cells still showed significant expression for *il-*
151 *1β*, *tnf-α and il-6* compared to untreated cells (Fig. 1f). This increased sensitivity was not present
152 to the same degree in the Tinaja cave population, since we only found an increase in the
153 expression of *il-6* (Fig. 1f).

154 This increased sensitivity of cavefish head kidney cells towards LPS *in vitro* is supported by
155 previous findings of an increased immune and scarring response after wounding of the Pachón
156 cavefish compared to surface fish[33]. However, the observed differences in the proinflammatory
157 response could be strongly affected by differences in the number of cells that produce these
158 proinflammatory cytokines. To account for this, we directly compared baseline expression of *il-*
159 *1β*, *tnf-α*, *il-6 and g-csf* in naïve head kidney cells of Pachón and Tinaja to surface fish (Fig. 1g).
160 Surprisingly, the expression of all tested proinflammatory cytokines was significantly reduced in
161 Pachón cavefish samples relative to surface fish cells (Fig. 1g). In the case of the proinflammatory
162 cytokine *il-1β*, for example, naïve Pachón cavefish head kidney cells produced 61 % less
163 transcript than surface fish cells (relative expression Pachón vs. surface fish *il-1β* = 0.383, $p \leq$
164 0.001*, pairwise fixed reallocation randomization test*, Fig. 1g). Similar to the Pachón cavefish
165 population, the Tinaja cave population differed in the expression of *il-1β*, *tnf-α* and *il-6* compared
166 to surface fish but not in the expression of *g-csf* (Fig. 1g). Here it is noteworthy that while we only

obtained parasite data from one cavefish population, we reasoned that different cave habitats share similar environmental features. To test whether functional differences of the immune system also appear in other cavefish populations we included, where it was feasible, a second, independently derived, cavefish population (Tinaja) in the experimental setup.

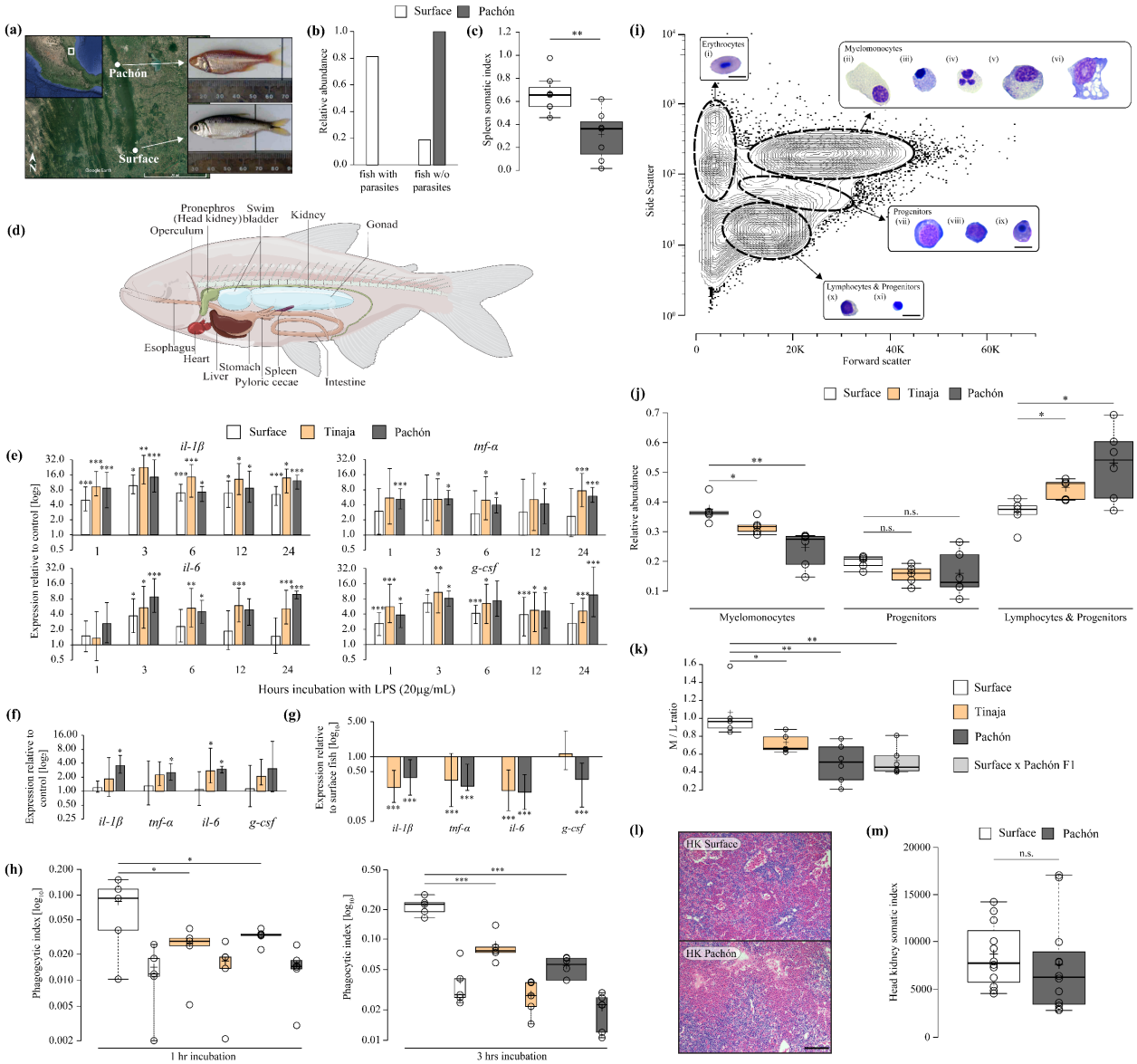

Figure 1: Adaptation to river and cave habitats with stark differences in parasite diversity result in changes of the proinflammatory response and immune investment strategy. *(***a**) Collection sites of *A. mexicanus* surface fish (Río Choy) and cavefish (Pachón). (**b**) Number of fish with and without visible ecto- and endoparasites. (**c**) Immune activity in wild surface and cavefish (n=7 for each) using the spleen somatic index, that is calculated by (weight [mg] (spleen) / weight [mg] (fish)) x 1,000. Significances were determined using a one-way ANOVA. (d) Cartoon of adult *A.*

mexicanus indicates anatomical position of the main hematopoietic and lymphoid organ, the head kidney (HK) that was used for subsequent in vitro experiments from surface fish and cavefish lab strains. (**e-f**) RT-qPCR analysis of pro-inflammatory cytokines, interleukin-1beta (*il-1β*), tumor necrosis factor alpha (*tnf-α*), interleukin-6 (*il-6*) and granulocyte colony stimulating factor (*g-csf*), of HK cells from surface fish and cavefish after incubation with (e) 20 µg/mL lipopolysaccharide (LPS) at various timepoints or (f) 0.2 µg/mL LPS after 24 hours relative to HK cells incubated without LPS for the given time point. Plotted is the mean of three independent experiments with standard error (SE) on a $\log_2$ scale. For all RT-qPCR results, PBS control samples from each time point and sample were used as the reference to calculate relative expression of target genes for each timepoint and fish, respectively. (**g**) RT-qPCR based expression analysis of proinflammatory cytokines *il-1β*, *tnf-α*, *il-6*, *g-csf* of cavefish relative to surface fish of naïve HK samples across all timepoints as shown in (e) (n=18). Significance values were determined by a pairwise fixed reallocation randomization test using REST2009 software. (**h**) Box plot presentation of relative phagocytic rate of HK cells from surface fish and cavefish incubated with Alexa-488 coupled *Staphylococcus aureus*. To control for passive uptake of Alexa-488 coupled *S. aureus*, a control sample was incubated with Alexa-488 coupled *S. aureus* in the presence of 80 µg cytochalasin B (CCB) and its phagocytic rate is presented in small boxes of the same color of the respective fish population and timepoint. Significant differences between surface fish (n=5), Tinaja (n=5) and Pachón (n=6) for each timepoint were determined by two-way Anova (see Table S2 for statistical details). (**i**) Representative contour plot of HK cells from three surface *A. mexicanus* after FACS analysis using scatter characteristics showing 99 % of all events. Four different populations (erythrocytes, myelomonocytes, progenitors and lymphocytes & progenitors) were identified and sorted for May-Grünwald Giemsa staining. Images of representative cells that were found in each population are shown for each population and identified based on similar approaches in zebrafish[31,32] as (i) mature erythrocytes, (ii) promyelocytes, (iii) eosinophiles, (iv) neutrophiles, (v) monocytes, (vi) macrophages, (vii) erythroblasts, (viii) myeloblasts, (ix) erythroid progenitors, (x) lymphocytes and (xi) undifferentiated progenitors. Scale bar is 10 µm. (**j**) Box plots of relative abundances of HK cells from surface and cavefish within the immune populations as defined by scatter characteristics in (**i**). Significances between surface (n=5), Tinaja (n=5) and Pachón (n=6) were determined by one-way ANOVA and subsequent FDR. (**k**) Box plot representation of myelomonocyte / lymphocyte (M / L) ratio from surface (n=5), Tinaja (n=5), Pachón (n=6) and surface x Pachón F1 hybrids (n=6). Significances were determined by one-way ANOVA and subsequent FDR. (**l**) H & E stained section of the head kidney from surface fish and Pachón cavefish (scale bar is 100 µm). (**m**) HK somatic index (mean number of head kidney cells per body weight [mg] fish) is shown for n=12 fish for surface fish and Pachón cavefish. Testing for significant differences was done using one-way ANOVA. For all box plots; center lines show the medians, crosses show means; box limits indicate the 25th and 75th percentiles as determined by R software; whiskers extend 1.5 times the interquartile range from the 25th and 75th percentiles, data points are represented by circles. Significances are indicated as * for $p \leq 0.05$; ** for $p \leq 0.01$ and *** for $p \leq 0.001$ for all experiments.

Given the difference in cytokine expression upon LPS exposure, we wanted to test whether other cellular immune functions, such as phagocytosis, differ between cavefish and surface fish. We conducted a phagocytosis experiment, in which we quantified the ability of head kidney cells to phagocytize Alexa-488 tagged *Staphylococcus aureus* cells (Thermo Fisher) *in vitro* at different timepoints (Fig. 1h, see Fig. S2 for gating strategy). Using pairwise comparison, we found a significant decrease of the phagocytic rate of both cavefish populations at both timepoints compared to surface fish (Fig. 1h, see Data File 1 for detailed statistic report).

The decreased baseline expression of the proinflammatory cytokines and the decreased phagocytosis rate in cavefish could be the result of changes in the immune cell composition, since both of these cellular immune functions are mainly fulfilled by cells with a myelomonocytic origin

221 (such as granulocytes and monocytes) in teleost fish[32,34,35]. To assess immune cell composition,
222 we analyzed scatter information from head kidney derived single cell suspensions from surface,
223 Tinaja and Pachón fish. Using similar analytical approaches previously described for
224 zebrafish[31,32], we identified four distinct cell cluster: an erythroid, a myelomonocyte, a progenitor
225 and a lymphoid/progenitor cluster (Fig. 1i). To confirm the identity of these clusters, head kidney
226 cells from each cluster were sorted, and cells were stained with May-Grünwald Giemsa stain.
227 Based on comparative morphological analysis[31,32], we identified (i) erythrocytes, (ii)
228 promyelocytes, (iii) eosinophiles, (iv) neutrophiles, (v) monocytes, (vi) macrophages, (vii)
229 erythroblasts, (viii) myeloblasts, (ix) erythroid progenitors, (x) lymphocytes and (xi)
230 undifferentiated progenitors (i.e. hematopoietic stem cells, common lymphoid progenitors and
231 common myeloid progenitors) within the four cell clusters (Fig. 1i). When we compared relative
232 abundances of the three immune cell clusters, we identified fewer myelomonocytic cells in both
233 cavefish populations (mean relative abundance of cells in myelomonocyte cluster in surface fish
234 is 0.37 vs. 0.32 in Tinaja, $p \leq 0.05$, and vs. 0.24 in Pachón, $p \leq 0.01$; one-way ANOVA, FDR
235 corrected; Fig. 1j) and an increased number of cells in the lymphocyte & progenitor cluster (mean
236 relative abundance of cells in lymphocyte & progenitor cluster in surface fish is 0.36 vs. 0.44 in
237 Tinaja, $p \leq 0.05$, and vs. 0.53 in Pachón, $p \leq 0.05$; one-way ANOVA; FDR corrected, Fig. 1j). We
238 used these relative abundances to calculate the myelomonocyte / lymphocyte (M / L) ratio. This
239 ratio is an indication of an individuals relative investment in either innate (myelomonocyte) or
240 adaptive (lymphocyte) immune cell populations[12,36].

241 We found profound differences in the immune investment strategy between surface fish and
242 cavefish. While surface fish have a relatively balanced investment in myelomonocyte and
243 lymphoid immune cells, cavefish invest less into myelomonocytic cells than into lymphoid immune
244 cell populations (mean M / L ratio in surface fish is 1.06 vs. 0.72 in Tinaja , $p \leq 0.05$, and vs. 0.50
245 in Pachón, $p \leq 0.01$; one-way ANOVA, FDR corrected, Fig. 1k). Since all fish were raised under

246 identical laboratory conditions, the observed differences in the immune investment strategy point
247 towards a genetic basis for this trait. To further study this, we analyzed surface x Pachón hybrids
248 and found a similar M / L ratio as in the parental Pachón population, indicating that the change in
249 the immune investment strategy of the Pachón population is a dominant trait (mean M/L ratio in
250 surface x Pachón F1 of 0.52, Fig. 1k).

251 Given the strong difference in parasite abundance and resource availibillity[25] between cave and
252 surface environments, cavefish potentially benefited from a change in the immune investment
253 that reduces the resource allocation into the immune system (see McDade, et al. [12] for review on
254 costs of innate and adaptive immune defences). To rule out the possibility that changes in the
255 head kidney morphology and / or total numbers of cells in the head kidney are responsible (and
256 could potentially compensate) for the observed differences in the M/L ratio, we compared
257 morphology and total cell numbers of the head kidney from surface fish and Pachón cavefish. We
258 observed no general differences in cell morphology (see Fig. 1l) and no significant changes in the
259 absolute cell number from the entire head kidney between the fish populations (mean absolute
260 cell number of entire head kidney per mg fish weight for surface fish was 8556 and 7460 for
261 cavefish, $p = 0.53$, one-way ANOVA; Fig. 1m).

262 To identify more specific differences in the immune cell composition of cavefish and surface fish,
263 we clustered head kidney cells based on cell morphological features using Image3C[37]. This tool
264 uses image-based flow cytometry and advanced clustering algorithms to cluster cells based on
265 their morphology and cellular features such as granularity of the cytoplasm or nucleus,
266 independent of an observer bias that has been reported for such analysis[38]. This makes it an
267 effective method for organisms lacking established transgenic lines or antibodies to identify
268 specific immune cell populations.

269

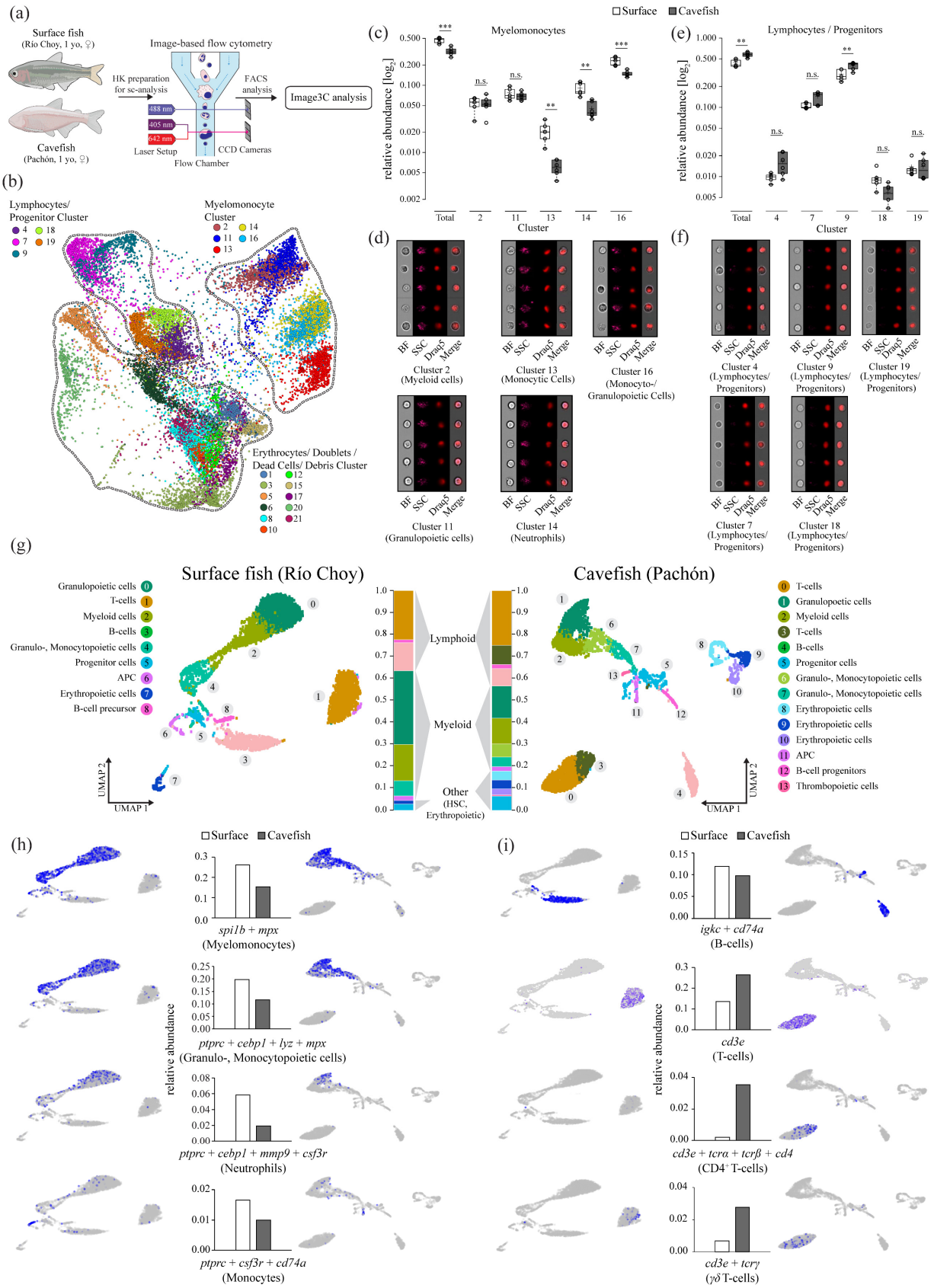
(a)
Surface fish
(Río Choy, 1 yo, ♀)
Cavefish
(Pachón, 1 yo, ♀)
Image-based flow cytometry
HK preparation for sc-analysis
FACS analysis
Image3C analysis
488 nm
405 nm
642 nm
Laser Setup
CCD Cameras
Flow Chamber
(b)
Lymphocytes/ Progenitor Cluster
Myelomonocyte Cluster
Erythrocytes/ Doublets / Dead Cells/ Debris Cluster
(c)
Myelomonocytes
relative abundance [log2]
Cluster
(d)
BF
SSC
Draq5
Merge
Cluster 2 (Myeloid cells)
Cluster 13 (Monocytic Cells)
Cluster 16 (Monocyto-/ Granulopoietic Cells)
Cluster 11 (Granulopoietic cells)
Cluster 14 (Neutrophils)
(e)
Lymphocytes / Progenitors
(f)
Cluster 4 (Lymphocytes/ Progenitors)
Cluster 9 (Lymphocytes/ Progenitors)
Cluster 19 (Lymphocytes/ Progenitors)
Cluster 7 (Lymphocytes/ Progenitors)
Cluster 18 (Lymphocytes/ Progenitors)
(g)
Surface fish (Río Choy)
Cavefish (Pachón)
Granulopoietic cells
T-cells
Myeloid cells
B-cells
Granulo-, Monocytopoietic cells
Progenitor cells
APC
Erythropoietic cells
B-cell precursor
Lymphoid
Myeloid
Other (HSC, Erythropoietic)
UMAP 1
UMAP 2
Granulo-, Monocytopoietic cells
Erythropoietic cells
B-cell progenitors
Thrombopoietic cells
(h)
Surface
Cavefish
spi1b + mpx (Myelomonocytes)
ptprc + cebp1 + lyz + mpx (Granulo-, Monocytopoietic cells)
ptprc + cebp1 + mmp9 + csf3r (Neutrophils)
ptprc + csf3r + cd74a (Monocytes)
relative abundance
(i)
igkc + cd74a (B-cells)
cd3e (T-cells)
cd3e + tcrα + tcrβ + cd4 (CD4+ T-cells)
cd3e + tcrγ (γδ T-cells)

270

Figure 2: Cell composition analysis of the head kidney of *A. mexicanus* surface and cave morphotypes using cell morphological and genetic features (**a**) Experimental setup for semi-unsupervised cell morphological clustering using the Image3C pipeline. (**b**) Force directed layout graph of cell clusters based on morphological feature intensities from HK cells of surface fish (n=5) and Pachón cavefish (n=6). Each dot represents a cell and each color represents a unique cluster. Clusters were combined into three categories (Myelomonocytes, Lymphocytes/Progenitors, mature Erythrocytes/Doublets/Debris) based on their morphology (see Data File 1 for cell galleries for each cluster). (**c**) Relative abundances of cells within each cluster of the myelomonocyte category with (**d**) image galleries of each cluster. (**e**) Relative abundances of cells within each cluster of lymphocyte/progenitor with (**f**) image galleries of each cluster. Significant differences in the relative abundance of cells within each category (total) or cluster were determined by one-way ANOVA and subsequent FDR. Significance values are indicated as ** for $p \leq 0.01$ and *** for $p \leq 0.001$. For box plots; center lines show the medians, crosses show means; box limits indicate the 25th and 75th percentiles as determined by R software; whiskers extend 1.5 times the interquartile range from the 25th and 75th percentiles, data points are represented by circles. Cell galleries show images of brightfield (BF), side scatter (SSC), nuclei (visualized through nuclei dye Draq5) and merged image of BF and Draq5 (Merge). (**g**) UMAP plot of single cell RNA sequencing analysis from one surface fish (Río Choy) and cavefish (Pachón) head kidney, respectively, where each dot represents a cell and each color represents unique cell cluster as shown in the legend. Overall relative abundances are given for each cluster shown in the respective color. (**h-i**) Relative abundance of specific cell populations of surface fish and cavefish and their location within UMAP representation of specific cell types from (h) myelomonocytes and (i) lymphocytes based on the expression of given gene(s). See Data File 3 for gene enrichment in each cluster.

First, we sorted myelomonocyte, lymphocyte and progenitor cell populations as identified in Fig. 1i in order to reduce mature erythrocytes from the single cell suspensions of head kidney cells (see Methods for details). In total, we recorded 10,000 cells by image cytometry from each replicate surface fish (Río Choy, n=5) and cavefish (Pachón, n=6) (Fig. 2a; see methods for more details) and identified 21 distinct cell clusters (Fig. 2b). The identity of each cluster was determined based on cell image galleries from each cluster (see Data File 2 for complete cell gallery) in comparison to the histological staining of sorted cells as presented in Fig. 1i. In addition, to verify certain cellular features (e.g., complexity of nuclei, cell shape, see Table S4 for feature details) within a certain cluster, we used a feature intensity/cluster correlation analysis (Fig. S3). Clusters were assigned to one of the following categories based on their morphological features: myelomonocytes (relatively large cells with medium to high granularity, irregular shaped nuclei and high cytoplasm to nuclei ratio; cluster 2, 11, 13, 14, 16); lymphocytes/progenitors (relatively small cells with low granularity and low cytoplasm to nuclei ratio; cluster 4, 7, 9, 18, 19) and mature erythrocytes/doublets/debris (cluster 1, 3, 5, 6, 8, 10, 12, 15, 17, 20, 21) (Fig. 2b). In line with the scatter analysis, we found a significant reduction of cells within the myelomonocyte category in cavefish compared to surface fish (mean relative abundance of 0.468 cells in surface fish vs 0.320 cells in cavefish; $p \leq 0.001$, one-way Anova and FDR correction, Fig. 2c).

308 More specifically, we identified differences in the relative abundance of monocytic cells (Fig. 2c-
309 d; relatively large cells with complex structured cytoplasm, high granularity and kidney shaped
310 nuclei; cluster 13; mean relative abundance of 0.021 cells in surface fish vs 0.006 cells in Pachón
311 cavefish; $p \leq 0.01$; one way ANOVA, FDR corrected), neutrophils (Fig. 2c-d; medium sized cells
312 with evenly distributed cytoplasm, high granularity and multi-lobed nuclei; cluster 14; mean
313 relative abundance of 0.088 cells in surface fish vs 0.044 cells in Pachón cavefish; $p \leq 0.01$ one
314 way ANOVA, FDR corrected) and monocytic-, granulocytic- and promyelocytic cells (Fig. 2c-d;
315 medium to large cells with high granularity; cluster 16; mean relative abundance of 0.231 cells in
316 surface fish vs 0.148 cells in Pachón cavefish; $p \leq 0.01$, one way ANOVA, FDR corrected)
317 between surface fish and cavefish.

318 The reduction of almost all myeloid cell populations suggests that there is an overall reduced
319 investment in the innate immune system in Pachón cavefish. The resulting reduction of
320 granulocytes and monocytes in cavefish head kidney is in line with the observed decreased
321 baseline expression of proinflammatory cytokines and phagocytic rate. Furthermore, we found
322 that cells within the lymphocyte/progenitor category (Fig. 2e-f) are generally overrepresented in
323 cavefish when compared to surface fish (mean relative abundance of cells within
324 lymphocytes/progenitor category: surface fish 0.433 vs. cavefish 0.580; $p \leq 0.01$ one-way Anova,
325 FDR corrected, Fig. 2e).

326 Most cluster in the lymphocytes/progenitor category did not differ significantly between surface
327 fish and cavefish with the exception of cluster 9 (surface fish 0.295 vs. cavefish 0.399; $p \leq 0.01$
328 one-way Anova, FDR corrected, Fig. 2e), which is the most abundant cluster in this category.
329 Here it is noteworthy, that the M/L ratio we obtained for surface and cavefish with the Image3C
330 approach is similar to the M/L ratio we obtained before (Fig. 1k) using standard scatter information
331 (M/L ratio surface 1.10 vs. 0.56 in Pachón, $p \leq 0.001$ one-way Anova, Fig. S4). However, given
332 the morphological similarities (see Data File 2) of early progenitor cells of hematopoietic lineages

333 and specific lymphocyte cell types (B-cells, T-cells), we were not able to further resolve the identity
334 of these cluster. Therefore, we took a genetic approach. We performed single-cell RNA
335 sequencing of head kidney cells, where mature erythrocytes were removed from the head kidney
336 cell suspension through FACS sorting as described above. We used one female adult surface
337 fish (Río Choy) and one age, size and sex- matched cavefish (Pachón). Using 10x genomics, we
338 captured 5874 surface fish HK cells and 4717 cavefish HK cells representing most hematopoietic
339 cell linages (Fig. 2g). Cluster identification was done using a comparative approach using gene
340 expression data from other teleost fish species (for details see Methods, Data File 3 for overall
341 gene enrichment in each cluster). Consistent with the morphological analyses, we found an
342 overall reduction in all cells of the myeloid linage in cavefish compared to surface fish. In detail,
343 cluster analysis revealed the reduction of myeloid cells (relative abundance of *spi1b* (*pu.1) + mpx*
344 cells in surface fish 0.221 vs. 0.132 in cavefish, Fig. 2h) and granulo- and monocytopoietic cells
345 (relative abundance of (*ptprc* + *cebp1* + *lyz* + *mpx* cells in surface fish 0.167 vs. 0.100 in Pachón
346 cavefish, Fig. 2h). Furthermore, we verified the reduction of mature neutrophils (relative
347 abundance of *ptprc* (*cd45*) + *cebp1* + *mmp9* cells in surface fish 0.0586 vs. 0.0191 in Pachón
348 cavefish, Fig. 2h) and monocytes (relative abundance of *ptprc* (*cd45*) + *csf3r* + *cd74a* cells in
349 surface fish 0.0165 vs. 0.010 in Pachón cavefish, Fig. 2h). Importantly, the analysis of the
350 lymphoid cell linage revealed that there are distinct differences in specific lymphoid cell
351 populations between cavefish and surface fish and not an overall increase in lymphoid cells in
352 cavefish as the morphological analysis might suggest (Fig. 2i).

353 While we found an over-representation in the relative abundance of lymphocytes in cavefish
354 compared to surface fish (Fig. 2g), we found almost identical relative abundances of B-
355 lymphocytes (relative abundance of *igkc* + *cd74a* cells in surface fish 0.119 vs. 0.098 in Pachón
356 cavefish). In contrast, we found clear differences in the numbers of HK resident T-cells (relative
357 abundance of *cd3e* cells in surface fish 0.136 vs. 0.265 in Pachón cavefish, Fig. 2i). We identified

358 increased numbers of CD4+ T-cells in cavefish (relative abundances of *cd3e* + tcr*α* + tcr*β* + *cd4-*
359 *1* in surface fish 0.002 vs 0.031 in Pachón cavefish, Fig. 2i). Interestingly, we observed that
360 $\gamma^{+}\delta^{+}$CD4^{-} CD8^{-} (*γδ*) T-cells reside in higher proportions in the headkidney of cavefish than in
361 surface fish (relative abundances of *cd3e* + *tcrγ* in surface fish 0.007 vs. 0.028 in Pachón cavefish,
362 Fig. 2i). *γδ* T-cells are a lymphoid cell population that potentially functions as a bridge between
363 the innate and adaptive immune system due to its ability to recognize antigens in an MHC-
364 independent manner[24] and has only been discovered recently in other teleost species[39].
365 Furthermore, *γδ* T-cells are reported to play a significant role in the development of autoimmune
366 diseases[23] and in homeostasis and inflammation of mammalian adipose tissue[40].

367 The changes in the immune investment strategy of cavefish suggests that the inflammatory
368 response of Pachón cavefish could be affected, since numbers of cells that drive proinflammatory
369 responses (monocytes and neutrophils) are decreased and cells that can promote homeostatsis
370 (*γδ* T-cells) are increased in Pachón cavefish. In addition, the dominance of the Pachón cavefish
371 immune investment phenotype suggests that there are genetic differences that drive these
372 changes. To address these questions we designed another scRNA-seq experiment (Fig. 3a). We
373 injected surface fish (Río Choy) and cavefish (Pachón) with either PBS or LPS and dissected the
374 head kidney 3 hours after injection (Fig. 3a). We removed the majority of mature erythrocytes
375 through FACS sorting as described before. Considering an unique molecular identifier count of ≥
376 500, we obtained a mean of 12,128 cells for each of the eight samples with a mean number of
377 667 genes per cell in each sample (Fig. 3a). With the increased numbers of cells per sample we
378 were able to resolve cellular identities at higher resolution as shown in Fig. 2g. As done before,
379 we mainly used cell-specific expression data from zebrafish to identify the identity of the single
380 cluster (for details see Methods section). We find higher numbers of myeloid cells in both
381 treatment groups of surface fish, which also resulted in higher numbers of granulopoietic
382 (granulocytes and their precursor cells) and monocytopoietic (monocytes and their precursor

383 cells) cell cluster (Fig. 3b). We were not able to identify a specific cluster of eosinophils, but this
384 is mainly due to the lack of a suitable genetic marker for this cell type. In contrast to the increased
385 numbers of myeloid cells in surface fish, we found an increased number of T-cells in both
386 treatment groups of cavefish similar to the previous experiment (see Fig. 3b and Fig. 2g). Again,
387 the increased numbers of cells per sample enabled a better resolution of the different T-cell
388 populations (Fig. 3b). Based on the gene expression profile, we found naïve T-cells, CD8 + T-
389 cells, Treg cells, CD4+ T-cells, and *γδ* T-cells in cavefish, while we only found naïve and CD4+
390 T-cells in surface fish (Fig. 3b and 3c). Even though we find T-cells with the same identity in
391 surface fish, the low numbers probably prevented clustering of these cells into a unique T-cell
392 cluster in surface fish. This underlines the differences in the immune investment strategy between
393 surface fish and Pachón cavefish, where surface fish invest more into innate immune cells and
394 Pachón cavefish more into adaptive, more specifically T-cells, immune cells.

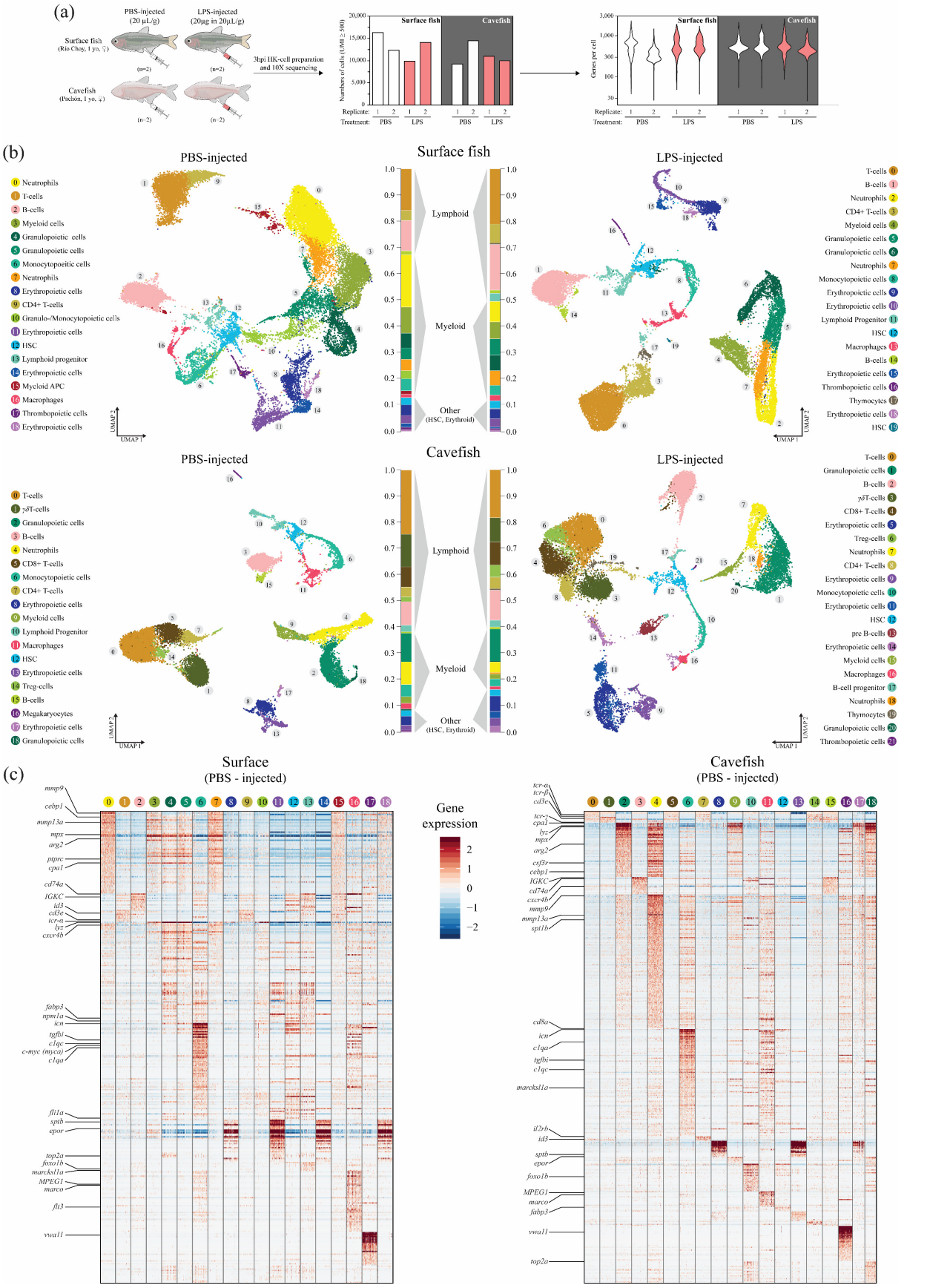
(a)
PBS-injected (20 µL/g)
LPS-injected (20µg in 20µL/g)
Surface fish (Rio Choy, 1 yo, ♀)
Cavefish (Pachón, 1 yo, ♀)
3hpi HK-cell preparation and 10X sequencing
Surface fish
Cavefish
Numbers of cells (UMI ≥ 500)
Genes per cell
Replicate:
Treatment:
PBS
LPS
(b)
PBS-injected
Surface fish
LPS-injected
Lymphoid
Myeloid
Other (HSC, Erythroid)
Cavefish
UMAP 1
UMAP 2
(c)
Surface (PBS - injected)
Cavefish (PBS - injected)
Gene expression

395

Figure 3: Cellular analysis of the acute inflammatory response upon LPS injection in head kidney cells of *A. mexicanus*. (**a**) Experimental setup of the scRNAseq experiment using head kidney from surface fish (Río Choy) and cavefish (Pachón) 3hrs post injection of either PBS or an LPS mix in given concentration. After processing, cells were sequenced using 10X Genomics technology (see Methods for details), which resulted in given cell numbers and average genes per cell. (**b**) UMAP projection of PBS and LPS injected surface and cavefish. Given cell cluster are based on gene enrichment analysis for each cluster. See Data File 4 for gene enrichment in each cluster. (**c**) Heatmap of enriched genes within each cell cluster of control groups from surface fish and cavefish. Genes that were used for cell cluster identification are shown. For a complete heatmaps for PBS and LPS injected groups see Data Files 5-8.

396 Given the previously observed differences in the immune investment strategy between surface
397 fish and cavefish, we speculated that these differences might be driven by genetic changes in
398 hematopoietic stem cells (HSCs). While we found no changes in the relative abundance of HSCs
399 across all samples (between 0.02 and 0.03, see Fig. 3b) we found distinct changes in the
400 transcriptional profiles of HSCs between surface fish and cavefish control samples that may affect
401 linage fate decision, the level of quiescence and self-renewal capacity (for a complete list of
402 differential expressed genes in HSC see Data File 9). For example we found that cavefish cells
403 show increased expression of *bcl3* (log2FC = 3.87), a marker for lymphoid progentitor cells[41], and
404 decreased expression of *npm1a* (log2FC = -1.22) and *mpx* (log2FC = -2.22), which are both key
405 marker for early myeloid progenitor cells[42,43]. While further genetical analysis is needed to verify
406 the genetic shift towards lymphoid progenitor cells in the cavefish HSCs, the transcriptional
407 changes suggest that the different immune investment strategies in *A. mexicanus* could indeed
408 be affected by genetic changes in cavefish HSCs. In addition, we found transcriptional changes
409 that indicate differences in self-renewal capacity and quiescence of HSCs between surface fish
410 and cavefish.

411 We detected increased expression of *c-myc* (*myca,* log2FC = 1.66) in cavefish cells, a positive
412 regulator of HSC quiescence and self-renewal[44]. Furthermore, we found genes, such as *fscna*
413 (log2FC = 3.056) and *pim1* (log2FC = 3.29), that are genetic marker for LT-(long-term) HSC
414 significantly increased and genetic marker, such as *top2a* (log2FC = -4.72), *kif2c* (log2FC = -4.04)
415 and *kif4* (log2FC = -3.05) for multipotent progenitor (MPP) cells significantly decreased in cavefish
416 control samples compared to surface fish controls[45]. Interestingly, we found no expression of

417 *cd34*, a common marker for mature HSCs and progenitor cells[46,47], in any of the Pachón HSC
418 cells, while we found expression of this marker in HSCs of the surface fish samples. Cd34
419 negative stem cells have been described as immature and quiescent with lower self- renewal
420 capacity[47]. These findings point towards an increased proportion of immature LT-HSC in a more
421 quiescent state in Pachón cavefish compared to surface fish.

422 Given the differences we observed in the lymphoid cell population structure between surface fish
423 and cavefish, we next looked for differences in the LPS response of the lymphoid fraction. The
424 expression of *interferon-γ* (*ifng*) of activated T-cells and Natural Killer (NK) cells is a well
425 established response upon bacterial or viral infection. Although Pachón cavefish posses a high
426 abundance of T-cells we found an increased abundance of *ifng* expressing cells in surface fish
427 (Fig. 4a,b, relative abundance of *ifng* expressing cells in surface fish 0.041 vs. 0.016 in cavefish;
428 for a complete list of differential expressed genes in the CD4+ T-cell cluster see Data File 10).

429 While we did not detect a specific NK-cell cluster in any of the treatment groups, we observed
430 that mainly CD4+ cells express *infg* in the acute pro-inflammatory response upon LPS injection.
431 We also compared the relative abundance of *ifng* expressing cells within the CD4+ T-cell cluster
432 and, again, found an increased abundance of *ifng* expressing cells in surface fish (Fig 4c, relative
433 abundance of *ifng* expressing cells in the CD4+ T-cell cluster in surface fish 0.43 vs. 0.26 in
434 cavefish). This decreased inflammatory response of CD4+ T-cells (Th1 response) in cavefish,
435 suggests that cavefish lymphoid cells possess a different mode of response than surface fish
436 upon bacterial recognition. Notably, we noticed a new activated B-cell population in LPS injected
437 Pachón fish that is absent in Pachón PBS treated groups and in both surface fish treatment groups

(Fig. 3b and 4a). The main charachteristic of this activated B-cell population is the expression of *foxo1b*, *rag-1* (Fig. 4a) and to a lesser extent *rag-2*, which is characteristic of activated B-cells[48,49].

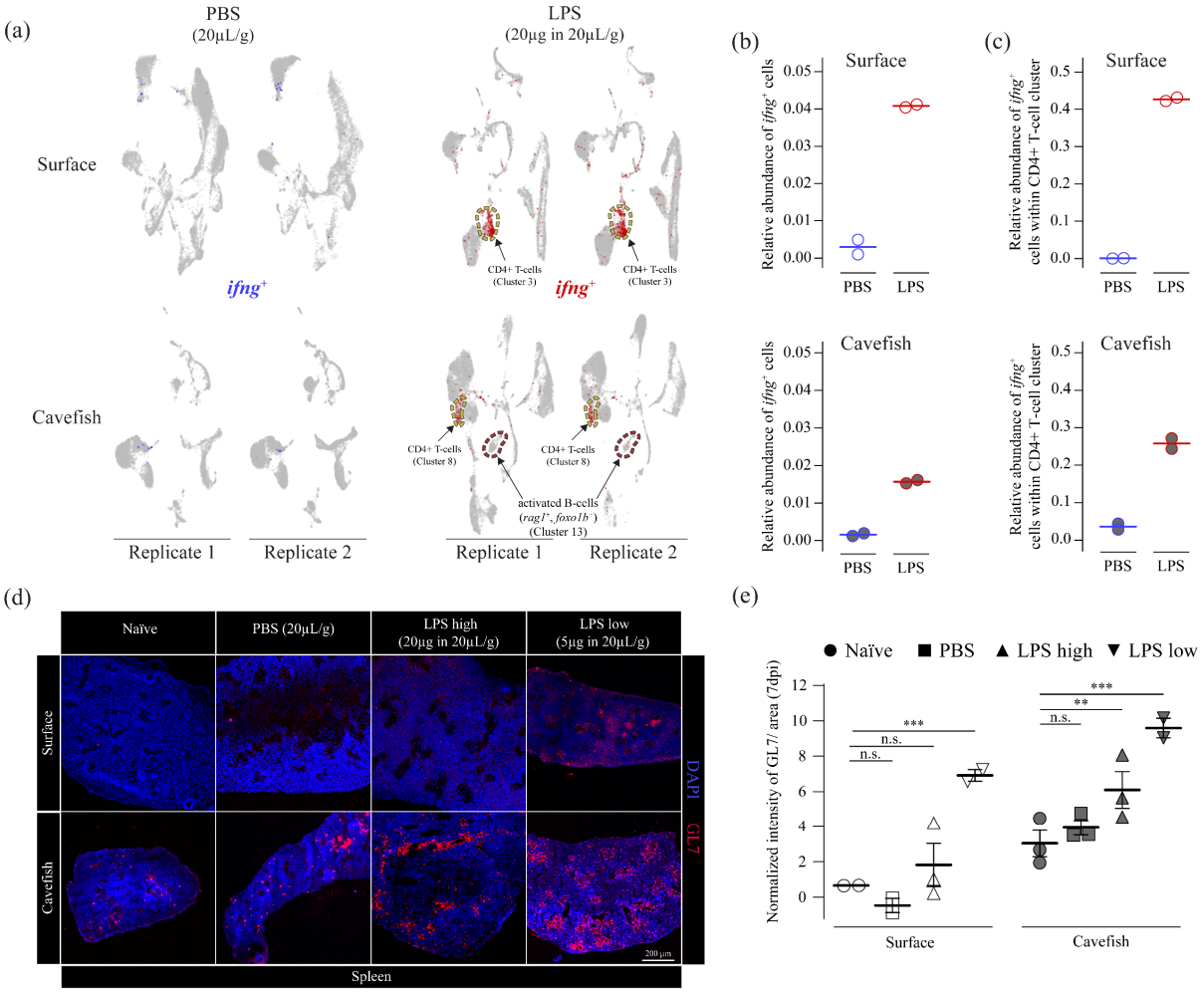

Figure 4: Adaptive response upon LPS injection in head kidney and spleen of surface and cavefish *A. mexicanus*. (a) *Interferon gamma* (*ifng*) expression 3hrs post PBS or LPS injection in head kidney cells. Upon LPS injection an activated B-cell cluster emerges in cavefish, which is absent in all other groups **(b)** Overall relative abundances for *ifng* expressing cells from scRNAseq experiment for each treatment group. **(c)** Relative abundances for *ifng* expressing cells from scRNAseq experiment within CD4+ T-cells for each treatment group. **(d)** Antibody staining (rat anti-GL7 Alexa Fluor® 647 (BD Pharmingen™) of activated B- and T-cells within germinal center of the spleen 7 days post injection (dpi) of either PBS (20µL/ g fish bodyweight), a high dose of LPS (LPS high; 20µg in 20µL/ g fish bodyweight) or a low dose of LPS (LPS low; 5µg in 20µL/ g fish bodyweight) or left naïve (not injected) as a control group. **(e)** Results of intensity analysis from (d) for 7 dpi. Images were analyzed from the 4 treatment groups from 2 timepoints (7 and 14 dpi, for 14 dpi analysis result see Figure S5) with n = 2-3 per treatment x population x timepoint sample. GL7 signal was quantified per area as defined by the DAPI signal using Fiji (see Methods for details) and intensities were normalized using the respective isotype control (see Methods for details). Empty symbols represent surface fish and filled symbols represent cavefish. A two-way ANOVA and subsequent multiple testing with FDR correction (Benjaminin-Hochberg) was used to detect differences between injected and control group (for complete statistical report see Data File 11). Significance values are indicated as ** for $p \leq 0.01$ and *** for $p \leq 0.001$.

457 Based on this, we hypothesized that Pachón cavefish display increased activation of B-cells after
458 injection with LPS compared to surface fish. To test this, we injected surface fish and Pachón
459 cavefish with either PBS (20µL/g), a high dose of LPS (20µg in 20µL/g) or with a low dose of LPS
460 (5µg in 20µL/g) or left naïve as control group and compared B- and T-cell activation status in the
461 spleen, a major lymphoid organ for antigen processing in teleost fish[50]. To visualize activated B-
462 cells we used an antibody against the GL-7 antigen that specifically stains activated B-cells that
463 respond to a T-cell dependent antigen immunization event in the germinal center of lymphoid
464 organs[51]. In surface fish we only found a significant increase of the GL-7 signal in the LPSlow
465 group compared to naïve group at 7dpi ($p \leq 0.0001$, multiple comparison after mixed effect
466 analysis, Fig. 4d and e, see Data File 11 for detailed statistical analysis). For cavefish, however,
467 we found significant increase of the GL-7 signal in the LPShigh and LPSlow group compared to
468 the naïve group at 7dpi ($p \leq 0.01$ and $p \leq 0.0001$, respectively, Fig. 5e and d). We did not find a
469 significant response upon LPS injection after 14dpi in surface and cavefish (see Fig. S5, see Data
470 File 11 for detailed statistical analysis). These findings indicate that Pachón cavefish mount a
471 more lymphoid (adaptive) driven immune response upon bacterial recognition than surface fish.

472 Finally, we asked whether the reduced investment into innate immune cells, such as granulocytes
473 and monocytes, in cavefish is accompanied by changes in gene expression of the
474 proinflammatory response (for a complete list of differential expressed genes in the neutrophil
475 and macrophage cluster see Data File 12 and 13, respectively). Here we found that the main
476 innate immune cells, neutrophils and macrophages, from cavefish showed increased expression
477 of *csf3r* (log2Fold = 2,85 and 1,14 compared to the surface fish PBS group, respectively).
478 Although we also found increased expression of the macrophage-associated colony stimulating
479 factor receptor (*csf1r*) in the cavefish control group compared to surface control fish, expression
480 was very low in all groups. However, the increased expression of *csf3r* in neutrophils and
481 macrophages indicates a higher sensitivity for its ligand *csf3* (*g-csf*), which is produced by a

482 variety of different immune cells to stimulate the release of Csf3r positive cells into the
483 bloodstream. We also found distinct changes in the inflammatory response in neutrophils and
484 macrophages of surface fish and cavefish upon injection with LPS. For example, components of
485 the NF-κB pathway, a major regulator of inflammatory processes in vertebrates[52], was
486 significantly increased in surface fish. However, based on the overall reduced investment of
487 cavefish into innate immune cells we asked whether there is also a reduction of cells that mediate
488 pro-inflammatory responses.

489 To test this, we used the expression of the cytokine *il-1β* as a readout, as this cytokine is described
490 as one major regulator of proinflammatory respones in teleost fish[53]. We detected induced
491 expression in granulopoietic cells (mainly mature neutrophils), monocytopoietic cells (mainly
492 mature monocytes) and macrophages in surface fish and cavefish upon LPS injection (Fig. 5a).
493 We found a 2.3 – fold increase of *il-1β* expressing cells in surface fish 3 hrs post LPS injection
494 compared to cavefish (mean overall relative abundance of cells expressing *il-1β* in surface fish
495 0.065 vs. 0.028 in cavefish, see Fig. 5b). Interestingly, cavefish seemed highly variable after PBS
496 injection (Fig. 5b), but when we compared expression of *il-1β* within each cell cluster, only
497 cavefish neutrophils showed elevated *il-1β* expression in both replicates of the PBS injected group
498 that is comparable to the induced expression after LPS injection (Fig. 5c). This, however, is a
499 cavefish neutrophil specific phenomenon since monocytopoietic cells (containing mature
500 monocytes) and macrophages do not express *il-1β* in the PBS injected Pachón samples (Fig. 5c).
501 It is noteworthy that macrophages from surface fish and cavefish showed the highest increase in

502 *il-1β* expressing cells and represent presumably the main producer of *il-1β* upon LPS injection in

503 *A. mexicanus* (Fig. 5c).

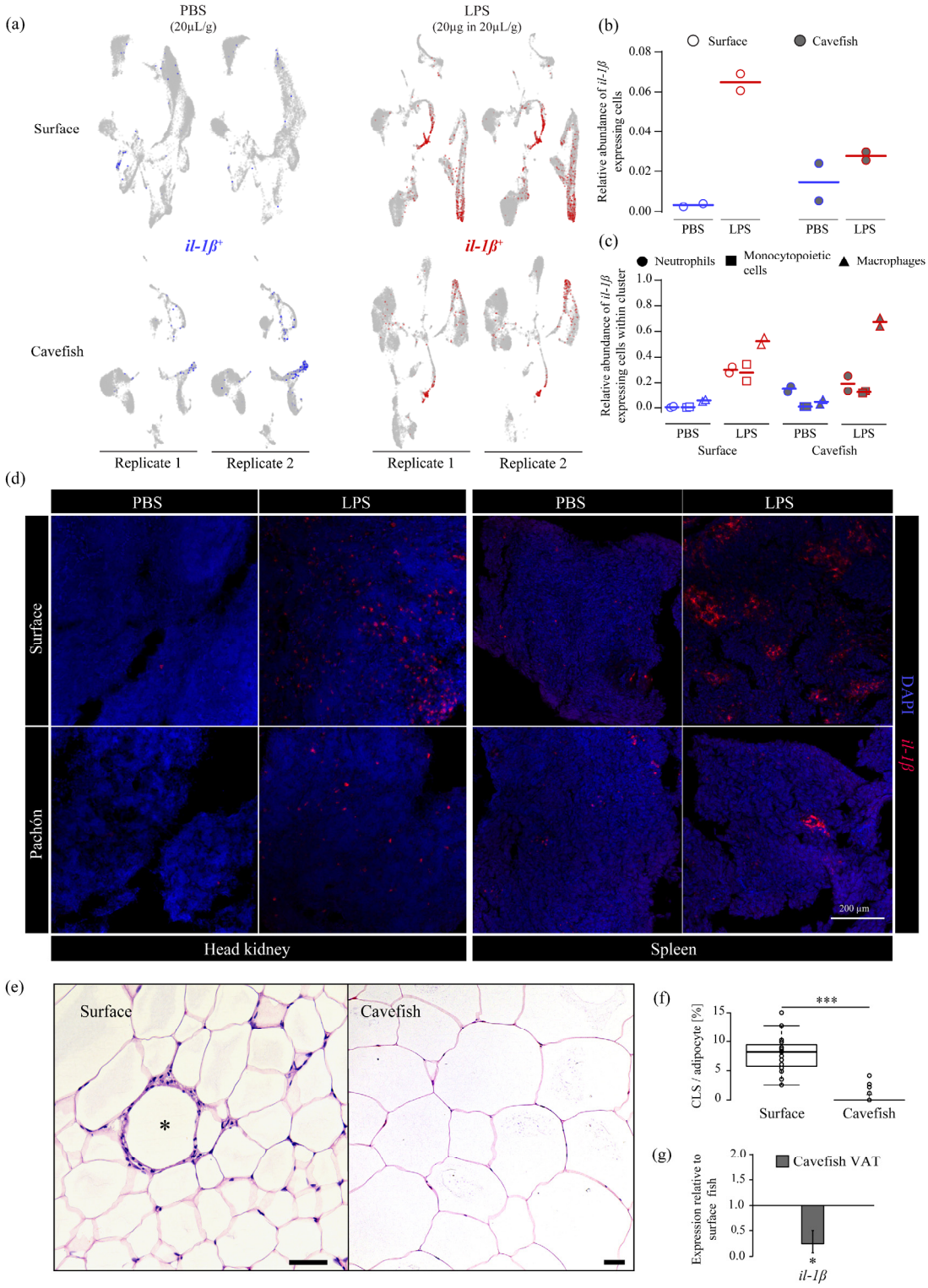

504

505 **Figure 5: Reduced immune investment into myeloid cells alters inflammatory and immunopathological**
506 **responses of *A. mexicanus*.** *(**a**) Interleukin-1ß* (*il-1ß*) expression 3 hrs post PBS or LPS injection in head kidney cells.
507 **(b)** Overall relative abundances of *il-1ß* expressing cells from scRNAseq experiment for each treatment group. **(c)**
508 Relative abundances of *il-1ß* expressing cells from scRNAseq experiment within the main *il-1ß* expressing cell cluster
509 for each treatment group. **(d)** *In-vivo* inflammatory response displayed by *in-situ* hybridyzation of *il-1β* using RNAscope
510 in head kidney and spleen of surface fish and cavefish 3 hours post intraperinoteal injection of 20µg in µL/g(bodyweight)
511 LPS. Images are representative of two independent experiments. Scale bar is 200 µm **(e)** H & E staining of visceral
512 adipose tissue (VAT) of surface fish and cavefish. Crown-like structure (CLS) is indicated as * in surface VAT. Scale
513 bar is 50 µm. **(f)** CLS count per 100 adipocytes in VAT of surface fish and cavefish in at least three fields of view for
514 each fish (n=3). Significance values were determined by one-way ANOVA. For all box plots; center lines show the
515 medians, crosses show means; box limits indicate the 25th and 75th percentiles as determined by R software; whiskers
516 extend 1.5 times the interquartile range from the 25th and 75th percentiles, data points are represented by circles.
517 Significance values are indicated *** for $p \leq 0.001$. **(g)** Gene expression of *il-1β* in cavefish VAT relative to surface fish
518 of the same fish that were used for (f). Significance values were determined by a pairwise fixed reallocation
519 randomization test using REST2009 software and are indicated as * for $p \leq 0.05$.

520

521 To verify the reduction in neutrophils and monocytes / macrophages that can initiate a
522 proinflammatory response, we designed an *in-situ* RNAscope probe for *il-1β* to visualize *il-1β*
523 expression in head kidney and spleen. We injected surface fish (Río Choy) and cavefish (Pachón)
524 with 20µg in 20µL/ g LPS and dissected head kidney and spleen 3 hours post injection (see
525 Methods section for details). In line with the scRNAseq analysis, LPS injected surface fish showed
526 an increased number of *il-1β* positive cells in the head kidney compared to cavefish (Fig. 5d). We
527 also detected considerably fewer cells that express *il-1β* after injection with LPS in the spleen
528 from cavefish compared to surface fish (Fig. 5d). In teleost fish, the spleen contains high numbers
529 of mononuclear phagocytes, e.g. macrophages[32,54] but is generally not a hematopoietic tissue for
530 such cell types [50]. In addition, we also used the *il-1β* RNAscope probe on dissociated head kidney
531 cells from surface fish 3 hrs post injection with LPS and we were able to validate that mainly cells
532 with monocytic and neutrophilic characteristics (multi-lobbed nuclei) express *il-1β* (Fig. S6).

533 Based on these results, we hypothesized that the lack of cells that initiate a systemic pro-
534 inflammatory response in cavefish upon exposure to an immune stimulant (e.g., LPS) could
535 potentially lead to a decreased presence of immunopathological phenotypes that result from such
536 pro-inflammatory responses. Cavefish produce substantially more visceral adipose tissue (VAT)
537 than surface fish[26]. In mammals, the amount of VAT is positively correlated with number of
538 monocytes infiltrating the adipose tissue and mediating inflammatory processes resulting in the

539 formation of crown-like structures (CLS)[55]. Therefore, we tested whether VAT of *A. mexicanus*
540 shows signs of CLS and if surface fish and cavefish differ in their occurrence. We detected CLS
541 in the visceral adipose tissue of surface fish (Fig. 5e), but not in cavefish, despite the prevalence
542 of large, hypertrophic adipocytes (average numbers of CLS in 100 adipocytes were 7.95 for
543 surface vs. 0.6 for cavefish, $p \leq 0.001$, one-way ANOVA, Fig. 5f). To measure levels of *il-1β*
544 expression, we took a sub-sample of the VAT for RT-qPCR analysis. We detected reduced
545 expression of *il-1β* in VAT of cavefish relatively to surface fish (mean relative expression of
546 cavefish compared with surface fish 0.249, $p \leq 0.05$, pairwise fixed reallocation randomization
547 test, Fig. 5g). In combination with the reduced number of crown-like structures, our data indicate
548 a reduction of pro-inflammatory granulocytes and macrophages in VAT of cavefish potentially
549 enabling increased VAT storage in cavefish without immunopathological consequences.

550

551 Conclusion

552 Our study elucidates how adaptation to low biodiversity in caves affects the immune investment
553 strategy of a vertebrate host. Besides differences in biodiversity, there are a variety of
554 environmental parameters that differ between the river and cave habitat (e.g. light conditions, food
555 availability, oxygen concentration). Differences in these parameters may potentially influence
556 different physiological systems that affect immune cell composition and function of *A. mexicanus*.
557 However, given that the maintenance and the control of the immune system is costly too[2], the
558 changes in the immune investment strategy of cavefish is likely an evolutionary response
559 facilitated by the low parasite diversity in the cave environment. Proinflammatory reactions are
560 one of the main causes for immunopathological phenotypes and have a tremendous impact on
561 the fitness of an organism and can be caused by a variety of environmental factors[56-58]. We
562 interpreted the reduction of innate immune cells in cavefish, which mediate proinflammatory
563 processes and act against parasites, as an adaptation decreasing auto-agressive

564 immunopathology from a hyper-sensitive immune system in an environment without parasite
565 diversity. With *A. mexicanus* we present a vertebrate system, which lost parasite diversity for
566 thousands of generations and presents immunological adaptations to such an environment that
567 prevent immunopathology.

568

569 Acknowledgements

570 We are grateful to the cavefish facility staff at the Stowers Institute for support and husbandry of
571 the fish. We would like to thank the staff from the Histology core at the Stowers Institute for their
572 technical support, Jillian Blanck from the Cytometry core for performing the sorting of head kidney
573 cells, Michael Peterson, Allison Peak and Anoja Perera for the scRNA-seq support, Mark Miller
574 for his support on the fish anatomy figure and Hua Li for her support on the statistical analysis.
575 Furthermore, we would like to thank Sean A. McKinney for providing the ImageJ macro for GL7
576 quantification. The authors also kindly acknowledge Joachim Kurtz for helpful discussions. NR
577 was supported by institutional funding, the Edward Mallinckrodt foundation and the JDRF. RP
578 was supported by a grant from the Deutsche Forschungsgemeinschaft (PE 2807/1-1).

579

580 Author Contributions

581 RP and NR conceived of the study. RP designed and coordinated the experiments with support
582 from ACB and JK. RP, JLP, AK and EM collected, dissected and examined cave and surface wild
583 populations with support from JPS. RP performed and analysed immune assays, flow cytometry
584 experiments and histological analysis with support from ACB, YW, DT and BPS. SC performed
585 single cell sequencing analysis with support from RP. RNAscope experiments and analysis were
586 performed by YW, DT and BPS with support from RP and JK. RP and NR designed and RP made
587 the figures. RP and NR wrote the paper and all authors read and edited the paper.

588

589 Data availability statement

590 Original data underlying this manuscript can be accessed from the Stowers Original Data
591 Repository at http://www.stowers.org/research/publications/libpb-1391. The scRNA-seq data
592 generated by Cell Ranger can be retrieved from the GEO database with accession number
593 GSE128306.

594

595 **Methods section**

596 Field sample collection

597 Collection for this study was conducted under permit No. SGPA/DGVS/03634/19 granted by the
598 Secretaría de Medio Ambiente y Recursos Naturales to Ernesto Maldonado. Study sites are
599 located in the Sierra de El Abra region of northeastern Mexico in the states of San Luis Potosí
600 and Tamaulipas. The El Abra region experienced repeated uplift and erosional events that carved
601 the underground limestone caverns (Mitchell, Russell, & Elliott, 1977). We collected samples from
602 Pachón cave; one of 30 caves in the region with known cave-dwelling *Astyanax* populations
603 (Espinasa et al., 2018; Mitchell et al., 1977). We also collected samples of the surface morphotype
604 from Nacimiento Río Choy approximately 95km south of Pachón cave.

605 We collected fish from Pachón cave and Nacimiento Río Choy on July 12th, 13th and 14th 2019
606 during the rainy season. Pachón fish were collected in the morning of July 12th using handheld
607 nets. Río Choy fish were collected during the day on July 13th and 14th using a combination of
608 handheld nets, net traps and a modified plastic bottle trap. Captured fish were placed in their
609 environmental water and euthanized on the day of capture.

610 Fish husbandry

611 Unless otherwise stated, all fish used for the experiments were adult female fish aged 12-16
612 months. Surface morphs of *Astyanax mexicanus* were reared from Mexican surface fish (Río
613 Choy) and cavefish originated from the Pachón and Tinaja cave. Fish were housed at a density
614 of ~ 2 fish per liter. The aquatic animal program at the Stowers Institute meets all federal
615 regulations and has been fully AAALAC-accredited since 2005. *Astyanax* are housed in glass fish
616 tanks on racks (Pentair, Apopka, FL) with a 14:10 h light:dark photoperiod . Each rack uses an
617 independent recirculating aquaculture system with mechanical, chemical and biologic filtration
618 and UV disinfection. Water (supplemented with Instant Ocean Sea Salt [Blacksburg, VA]) quality
619 parameters are maintained within safe limits (Upper limit of total ammonia nitrogen range, 1 mg/L;
620 upper limit of nitrite range, 0.5 mg/L; upper limit of nitrate range, 60 mg/L; temperature, 22 °C;
621 pH, 7.65; specific conductance, 800 µS/cm; dissolved oxygen 100 %). Fish were fed once per
622 day with mysis shrimp and twice per day with Gemma diet (according to the manufacturer is
623 Protein 59%; Lipids 14%; Fiber 0.2%; Ash 14%; Phosphorus 1.3%; Calcium 1.5%; Sodium 0.7%;
624 Vitamin A 23000 IU/kg; Vitamin D3 2800 IU/kg; Vitamin C 1000 mg/kg; Vitamin E 400 mg/kg) at
625 a designated amount of approximately 3% body mass. Routine tank side health examinations of
626 all fish were conducted by dedicated aquatics staff twice daily. *Astyanax* colonies are screened
627 at least biannually for *Edwardsiella ictaluri, Mycobacterium spp., Myxidium streisingeri,*
628 *Pseudocapillaria tomentosa, Pseudoloma neurophilia*, ectoparasites and endoparasites. At the
629 time of the study, none of the listed pathogens were detected.

630
631 *In-vitro* gene expression analysis

632 Single cell suspensions from freshly dissected head kidney tissue were produced by forcing tissue
633 through 40 µM cell strainer into L-15 media (Sigma), containing 10 % water and 5 mM HEPES
634 buffer (pH 7.2) and 20 U/mL heparin (L-90). The strainer was washed once with L-90 and cells
635 were washed once by spinning cells at 500 x *g* at 4 ºC for 5 mins. Supernatant was discarded

636 and cells were resuspended in 1 mL of L-90 media (L-15 containing 10 % water, 5 mM HEPES
637 (7.2 pH), 5 % fetal calf serum, 4 mM L-glutamin, Penicillin-Streptomycin mix with 10,000 U/mL
638 each). Cells were counted using EC800 analyser (Sony Biotechnology) and $1x10^6$ cells were
639 plated in 48 well plate in 500 µL and incubated over night at 21 ºC. At timepoint 0, 20 µg / ml or
640 0.2 µg / mL lipopolysaccharide mix in PBS (*Escherichia coli* O55:B5 and *E. coli* O111:B4, 1 mg/mL
641 each) or PBS alone as a control was added to the cells, respectively. After 1, 3, 6, 12 and 24
642 hours, cells were harvested and immediately snap frozen in liquid nitrogen and RNA was isolated
643 as described previously[59]. 100 ng of RNA (concentration was measured using the Qubit system
644 (Thermo Fisher)) from each sample was used for cDNA synthesis using the SuperScript™ III
645 First-Strand Synthesis System kit (Invitrogen) following manufacturer instructions. Resulting
646 cDNA was used for RTqPCR using the PerfeCTa® SYBR® Green FastMix® (Low ROX)
647 (Quantabio) following manufacturer instructions. Gene specific primers (see Table S1) were used
648 for amplification of target and the two housekeeping genes (rpl32 and rpl13a, see Table S1 for
649 details). Where possible, gene specific primers were designed to span an exon – exon junction.
650 Samples were pipetted in a 384 well plate using a Tecan EVO PCR Workstation (Tecan) and
651 samples were run in technical triplicates on a QuantStudio 7 Flex Real-Time PCR System
652 (Thermo Fisher). Quality control for each sample was performed using the QuantStudio Real-
653 Time PCR software (Thermo Fisher) and data was exported for analysis in REST 2009[60] as
654 described before[59]. PBS control samples from each time point and sample was used as the
655 reference to calculate relative expression of target genes for each timepoint and fish, respectively.

656

657 Phagocytosis Assay

658 Phagocytosis was measured as previously described[61]. Briefly, a single cell solution from freshly
659 dissected head kidney tissue was prepared as described above and $4x10^5$ cells were pipetted
660 into 96 well flat bottom plate and Alexa-488 tagged *Staphylococcus aureus* (Thermo Fisher) were

661 added in a 1:50 cells / bacteria ratio. To control for cell viability a sample without bacteria was
662 included and to control for active phagocytosis a sample with cells containing bacteria and
663 cytochalasin B (CCB) (0.08 mg /mL) for each individual sample was included. Cells were
664 incubated in 200 µL of L-90 media at 21 ºC for 1 and 3 hours, respectively. To exclude dead cells
665 and signal from non-phagocytosed particles, cells were stained with Hoechst and all samples
666 were quenched using 50 µL Trypan Blue (0.4 % solution, Sigma) before the measurement.
667 Samples were measured on EC800 Analyzer (Sony Biotechnology). Cells were gated for live and
668 Alexa-488 positive and phagocytosis rate was calculated as the ratio of live (Hoechst positive,
669 Excitation 352 nm, Emission 461 nm, FL-6) and phagocytes (Alexa-488 positive, Excitation 495
670 nm, Emission 519 nm, FL-1) vs. live cells.

671

672 Scatter analysis of head kidney

673 Single cells from head kidney from adult surface fish were extracted as described above. Cells
674 were stained with DAPI to exclude dead cells and live cells were sorted based on populations as
675 described in Fig. 1i using forward side scatter and side scatter characteristics of cells using an
676 Influx System (BD). 1000 cells per population were sorted on a Thermo Scientific™ Shandon™
677 Polysine Slides and incubated for 30 min at 21 ºC, so cells could settle and adhere to slides. Cells
678 were then fixed with 4 % Paraformaldehyde and washed three times in PBS. Cells were then
679 stained using May-Grünwald Giemsa protocol. Briefly, slides were stained for 10 min with a 1:2
680 solution of May-Grünwald (made in phosphate buffer pH 6.5, filtered), the excess stain was
681 drained off and slides were stained 40 min with a 1:10 solution of Giemsa (made in phosphate
682 buffer pH 6.5, filtered). Then slides were rinsed in ddH_20 by passing each slide under running
683 ddH_20 10 times. For differentiation, a drop of 0.05 acid water (5ml glacial acetic acid/95ml ddH_2O)
684 was put on slide for approx. 4 seconds and quickly rinsed off. Slides were rinsed well, air dried

685 and coverslipped. Only cells that could clearly be identified based on studies in closely related
686 organisms using a similar approach[30,32] were used as representative image for Fig. 1i.

687

688 Image-based cluster analysis of head kidney

689 For this analysis, hematopoietic cells from the head kidney were presorted to remove the mature
690 erythrocyte cluster using the S3 Cell Sorter (Bio-Rad) using scatter features (as in Fig. 1i). This
691 was necessary since mature erythrocytes account for about 8 % and 7 % respectively in surface
692 fish and Pachón fish of the entire cell count in the head kidney based on the erythrocyte population
693 we were able to identify using scatter alone (see Fig. 1i). However, based on their biconcave
694 morphology we found erythrocytes in all populations that we could separate through scatter,
695 although mainly in the myelomonocytic and progenitor populations to different degrees since
696 different orientations in the flow cell of erythrocytes result in different morphological shapes[37].
697 Based on this, the presence of mature erythrocytes results in massive over-clustering[37].
698 Reduction of erythrocytes through sorting based on scatter can be used to reduce the amount of
699 over-clustering using the pipeline[37]. Sorted cells were stained with 5 µM Draq5 and 10,000
700 nucleated, single events were acquired from samples on the ImageStream®X Mark II at 60x, slow
701 flow speed, using 633 nm laser excitation. Bright field was acquired on channels 1 and 9 and
702 Draq5 on channel 11. SSC was acquired on channel 6. Intensities from 25 unique morphological
703 features were extracted. Further analysis was done as described before[37].

704

705 Intraperitoneal injection of LPS

706 Fish were individualized and fasted the day before the treatment (naïve, PBS-injected or LPS
707 injected). After 24hrs the fish were anesthetized using ice cold system water and either PBS
708 (20µL/g bodyweight) or a LPS mix (*E. coli* O55:B5 and *E. coli* O111:B4, 20µg or 5µg in 20 µL/g

709 bodyweight) was injected intraperitoneally using an insulin syringe (3/10 mL, 8 mm length, gauge
710 size 31G, BD). After given timepoints, fish were euthanized using buffered Tricaine solution (500
711 mg/L) and respective organs were dissected and were either dissociated (single cell RNA
712 sequencing) or immediately fixed in 4 % paraformaldehyde / DEPC water (RNAscope analysis)
713 for subsequent analysis.

714

715 Single cell RNAseq

716 Dissociated hematopoietic cells were stained with DAPI to exclude dead cells and live cells were
717 sorted based on populations as described in Fig. 1i, where only myelomonocyte, lymphocyte and
718 progenitor populations were sorted in L-90 media, to reduce the relative abundance of mature
719 erythrocytes. Sorted cells were spun down (500 x rcf, 4º C, 5 min), supernatant was discarded,
720 and cells were resuspended in L-90 media and run again on Influx system to ensure removal of
721 mature erythrocyte cluster and measure cell viability (percentage live cells after sorting: surface
722 fish 82.2 % and cavefish 88.9 %). Cells were loaded on a Chromium Single Cell Controller (10x
723 Genomics, Pleasanton, CA), based on live cell concentration, with a target of 6,000 cells per
724 sample. Libraries were prepared using the Chromium Single Cell 3' Library & Gel Bead Kit v2
725 (10x Genomics) according to manufacturer's directions. Resulting short fragment libraries were
726 checked for quality and quantity using an Agilent 2100 Bioanalyzer and Invitrogen Qubit
727 Fluorometer. Libraries were sequenced individually to a depth of ~330M reads each on an Illumina
728 HiSeq 2500 instrument using Rapid SBS v2 chemistry with the following paired read lengths: 26
729 bp Read1, 8 bp I7 Index and 98 bp Read2. Raw sequencing data were processed using 10X
730 Genomics Cell Ranger pipeline (version 2.1.1). Reads were demultiplexed into Fastq file format
731 using cellranger mkfastq. Genome index was built by cellranger mkref using cavefish genome
732 astMex1, ensembl 87 gene model. Data were aligned by STAR aligner and cell counts tables
733 were generated using cellranger count function with default parameters. Cells with at least 500

734 UMI counts were loaded into R package Seurat (version 2.3.4) for clustering and trajectory
735 analysis. 4991 cells for surface and 4103 cells for Pachón cavefish were used for downstream
736 analysis. The UMI count matrix were log normalized to find variable genes. First 12 principal
737 components were selected for dimension reduction and t-SNE plots. Marker genes were used to
738 classify clusters into lymphocytes, myelomonocytes and progenitor types. The results generated
739 by Cell Ranger can be retrieved from the GEO database with accession number GSE128306.
740 The assignment of cell identities is based on their transcription profile determined by similar
741 approaches in zebrafish[32,62-65].

742

743 Single-cell RNAseq for LPS injection

744 Libraries were sequenced paired-end using Illumina Novaseq S2 flowcell. Raw data were
745 processed using Cell Ranger pipeline (version 3.0) and demultiplexed into Fastq file format using
746 cellranger mkfastq. Data were aligned to astMex1, ensemble 87 gene model by STAR aligner
747 and cell counts tables were generated using cellranger count function with default parameters.
748 Cells with at least 500 UMI counts were loaded into R package Seurat (version 3.0) for clustering
749 and trajectory analysis. The UMI count matrix were log normalized to find top 2000 variable genes
750 using vst selection method from Seurat. Replicates were then integrated using SCTtransform
751 function FindIntegrationAnchors based on Seurat's vignettes. Principal components cutoffs were
752 selected based on Jackstraw and Elbowplot function for dimension reduction and UMAP plots.
753 De novo markers genes were generated using FindAllMarkers function and to plot heatmaps in
754 Figure 3. Trajectory analysis were computed using R package slingshot. All scRNA-seq data can
755 be retrieved from the GEO database with accession number GSE128306.

756

757 *Il-1β* RNAscope assay

758 Section preparation and RNA in situ hybridization were performed as previously reported[26,66].
759 Briefly, for tissue section, respective tissues (head kidney, spleen) were dissected from surface
760 fish and cavefish, followed by immediate immersion into 4% PFA in DEPC H_2O (diluted from 16%
761 (wt/vol) aqueous solution, Electron Microscopy Sciences, cat# 15710) for 24hr at 4°C to fix the
762 tissue, then rinsed well with 1xPBS, dehydrated through graded ethanol (30%, 50%, 70%) and
763 processed with a PATHOS Delta hybrid tissue processor (Milestone Medical Technologies, Inc,
764 MI). Paraffin sections with 8 µm thickness were cut using a Leica RM2255 microtome (Leica
765 Biosystems Inc. Buffalo Grove, IL) and mounted on Superfrost Plus microscope slides (cat# 12-
766 550-15, Thermo Fisher Scientific). For single cell solutions, head kidney and spleen were
767 dissected, and single cell solutions were produced as described above and approx. 20 µL of the
768 suspension was pipetted on Superfrost Plus microscope slides (cat# 12-550-15, Thermo Fisher
769 Scientific). Cells were allowed to settle for 30 min and fixed using 4% PFA (diluted from 16%
770 (wt/vol) aqueous solution, Electron Microscopy Sciences, cat# 15710) for 1hr at RT, then rinsed
771 well with 1XPBS, dehydrated through graded ethanol (30%, 50%, 70%). RNA in situ hybridization
772 was performed using RNAscope multiplex fluorescent detection V2 kit according to the
773 manufacturer's instructions (Advanced Cell Diagnostics, Newark, CA). RNAscope probe for *il-1β*
774 was a 16ZZ probe named Ame-LOC103026214- C2 targeting 217-953 of XM_022680751.1.

775 Images of sections were acquired on a Nikon 3PO spinning disc on a Nikon Ti Eclipse base,
776 outfitted with a W1 disk. A 0.75 NA, Plan Apochromat Lambda 20x air objective was used. DAPI
777 and AF647 were excited with a 405 nm and 640 nm laser, respectively, with a 405/488/561/640
778 nm main dichroic. Emission was collected onto an ORCA-Flash 4.0 V2 digital sCMOS camera,
779 through a 700/75 nm and 455/50 nm filter for the far-red channel and DAPI channel, respectively.
780 Z-step spacing was 1.5 microns. All microscope parameters and acquisition were controlled with
781 Nikon Elements software. Identical camera exposure time and laser power was used across
782 samples. All image processing was done with an open source version of FIJI[67] with standard

783 commands. A Gaussian blur with radius of 1 was applied and a rolling ball background subtraction
784 with a radius of 200 pixels was applied to every channel with the exception of the DAPI channel.
785 Following that, a max projection across the slice was applied. For direct comparison, images
786 shown are contrasted identically in the far red channel (*il-1β*).

787

788 GL-7 analysis of spleen after LPS injection

789 Fish were dissected 3hrs after treatment and the spleen was immediately embedded with OCT
790 compound (Tissue-Tek, CA) and freezed at -70°C. Cryo sections with 12μm thickness were cut
791 using a Leica CM3050S cryostat (Leica Biosystems Inc. Buffalo Grove, IL) and mounted on glass
792 slides. Sections were kept in cyrostat for 2hr before fixed with pre-chilled 75% acteone/25%
793 ethynoal at room temprature for 30 min. Immunofluorescence assay was performed manually
794 using an Alexa Fluor 647 conjugated rat anti-mouse T-cell and B-cell activation antigen (BD
795 Pharmingen, GL7 clone, cat# 561529) and a matched isotype control (BD Pharmingen, R4-22
796 clone, cat# 560892). Here, IF experiments were repeated three times with different populations
797 and timepoints, which accumulated a total number of 48 animals. In brief, sections were
798 rehydrated with 1X PBS and background was blocked by incubating sections in Background
799 Buster solution (NB306, Innovex Biosciences, CA, USA) for 30 min. The antibody was diluted
800 1:500 in Antibody Diluting Reagent (003118, Invitrogen, Carlsbad, CA, USA) and incubated
801 overnight at 4°C. Sections were further stained with DAPI (1:1000) for 10min, and then washed
802 in tris-buffered saline (25 mM Tris, 0.15 mM NaCl, pH7.2) with 0.05% Tween-20 (TBST) and
803 coverslipped before imaging. Images of sections were acquired on a Zeiss LSM 700 upright
804 microscope. A 5x air objective was used. DAPI and AF647 were excited with a 405 nm and 640
805 nm laser, respectively, with a 405/488/561/640 nm main dichroic. Emission was collected onto an
806 ORCA-Flash 4.0 V2 digital sCMOS camera, through a 700/75 nm and 455/50 nm filter for the far-
807 red channel and DAPI channel, respectively. All image processing was done with an open source

808 version of FIJI[67] with standard commands. For GL-7 intensity analyis we used Fiji macro that is
809 publicly available under https://github.com/jouyun/smc-
810 macros/blob/master/ROP_IntensityMeasurement.ijm.

811

812 Visceral adipose tissue analysis

813 We dissected the visceral adipose tissue (VAT) from the abdominal cavity as described
814 previously[26]. In short, we manually removed the intestinal sack of the fish and carefully isolated a
815 piece of fat tissue located around the gut for RTqPCR as described above. The rest of the sample
816 was immediately fixed in 4% paraformaldehyde for 18 h at 4 °C and embedded in JB-4 Embedding
817 solution (Electron Microscopy Sciences; #14270-00) while following kit instructions for
818 dehydration, infiltration and embedding. After sectioning at 5 µm, we dried slides for 1 h in a 60
819 °C oven and stained slides with hematoxylin for 40 min. After rinsing the slides in PBS, semi-dried
820 slides were stained with eosin (3% made in desalted water) for 3 min. Slides were washed with
821 desalted water and air dried. At least 3 images from VAT of each fish were taken at similar location
822 around the gut and crown-like structures were scored as described previously[68]. Images were
823 obtained using a 10X objective on Zeiss Axioplan2 upright microscope and adipocytes and CLS
824 were counted using Adobe Photoshop CC (Version 19.1.0).

825

826 Statistical Analysis

827 Graphical data and statistics were produced using R[69] except otherwise stated. For comparisons
828 between populations we used a one-way ANOVA and corrected for multiple testing against the
829 same control group (FDR) with Benjamini-Hochberg test[70]. For analysis of RT-qPCR data we
830 used the REST2009 software where significant differences between two groups were determined
831 by a pairwise fixed reallocation randomization test[60]. Two-way ANOVA analysis was done using

832 Graph Pad Prism Software (Version 8.0.2). Multiple testing against the same control group was
833 corrected with FDR test Benjamini-Hochberg test[70]. To determine significant differences of
834 morphological cell cluster between surface fish and cavefish that resulted from X-shift clustering[71]
835 we used a negative binominal regression model as described before[37].
836
837 Animal experiment statement

838 Research and animal care were approved by the Institutional Animal Care and Use Committee
839 (IACUC) of the Stowers Institute for Medical Research.
840

841 **References**

842

843 1 WHO. *The global burden of disease: 2004 update.*, (2004).
844 2 Sheldon, B. C. & Verhulst, S. Ecological immunology: costly parasite defences and trade-
845 offs in evolutionary ecology. *Trends in Ecology & Evolution* **11**, 317-321 (1996).
846 3 Schmid-Hempel, P. Variation in immune defence as a question of evolutionary ecology.
847 *Proceedings. Biological sciences* **270**, 357-366 (2003).
848 4 Rook, G. A. Regulation of the immune system by biodiversity from the natural
849 environment: an ecosystem service essential to health. *Proceedings of the National*
850 *Academy of Sciences of the United States of America* **110**, 18360-18367 (2013).
851 5 von Hertzen, L., Hanski, I. & Haahtela, T. Natural immunity. Biodiversity loss and
852 inflammatory diseases are two global megatrends that might be related. *EMBO reports*
853 **12**, 1089-1093 (2011).
854 6 Belkaid, Y. & Hand, T. W. Role of the microbiota in immunity and inflammation. *Cell* **157**,
855 121-141 (2014).
856 7 Lambrecht, B. N. & Hammad, H. The immunology of the allergy epidemic and the hygiene
857 hypothesis. *Nature immunology* **18**, 1076-1083 (2017).
858 8 Rook, G. A., Martinelli, R. & Brunet, L. R. Innate immune responses to mycobacteria and
859 the downregulation of atopic responses. *Current opinion in allergy and clinical immunology*
860 **3**, 337-342 (2003).
861 9 Rosenblum, M. D., Remedios, K. A. & Abbas, A. K. Mechanisms of human autoimmunity.
862 *J Clin Invest* **125**, 2228-2233 (2015).
863 10 Lafferty, K. D. Biodiversity loss decreases parasite diversity: theory and patterns.
864 *Philosophical transactions of the Royal Society of London. Series B, Biological sciences*
865 **367**, 2814-2827 (2012).
866 11 Kamiya, T., O'Dwyer, K., Nakagawa, S. & Poulin, R. Host diversity drives parasite
867 diversity: meta-analytical insights into patterns and causal mechanisms. *Ecography* **37**,
868 689-697 (2014).
869 12 McDade, T. W., Georgiev, A. V. & Kuzawa, C. W. Trade-offs between acquired and innate
870 immune defenses in humans. *Evolution, medicine, and public health* **2016**, 1-16 (2016).

13 Lindstrom, K. M., Foufopoulos, J., Parn, H. & Wikelski, M. Immunological investments reflect parasite abundance in island populations of Darwin's finches. *Proceedings. Biological sciences* **271**, 1513-1519 (2004).
14 Mayer, A., Mora, T., Rivoire, O. & Walczak, A. M. Diversity of immune strategies explained by adaptation to pathogen statistics. *Proceedings of the National Academy of Sciences of the United States of America* **113**, 8630-8635 (2016).
15 Scharsack, J. P., Kalbe, M., Harrod, C. & Rauch, G. Habitat-specific adaptation of immune responses of stickleback (Gasterosteus aculeatus) lake and river ecotypes. *Proceedings. Biological sciences* **274**, 1523-1532 (2007).
16 Kaczorowski, K. J. *et al.* Continuous immunotypes describe human immune variation and predict diverse responses. *Proceedings of the National Academy of Sciences of the United States of America* **114**, E6097-E6106 (2017).
17 Herman, A. *et al.* The role of gene flow in rapid and repeated evolution of cave-related traits in Mexican tetra, Astyanax mexicanus. *Molecular ecology* **27**, 4397-4416 (2018).
18 Fumey, J. *et al.* Evidence for late Pleistocene origin of Astyanax mexicanus cavefish. *BMC evolutionary biology* **18**, 43 (2018).
19 Gibert, J. & Deharveng, L. Subterranean Ecosystems: A Truncated Functional Biodiversity. *BioScience* **52** (2002).
20 Tabin, J. A. *et al.* Temperature preference of cave and surface populations of Astyanax mexicanus. *Developmental biology* **441**, 338-344 (2018).
21 Abolins, S. *et al.* The comparative immunology of wild and laboratory mice, Mus musculus domesticus. *Nature communications* **8**, 14811 (2017).
22 Trama, A. M. *et al.* Lymphocyte phenotypes in wild-caught rats suggest potential mechanisms underlying increased immune sensitivity in post-industrial environments. *Cellular & molecular immunology* **9**, 163-174 (2012).
23 Paul, S., Shilpi & Lal, G. Role of gamma-delta (gammadelta) T cells in autoimmunity. *Journal of leukocyte biology* **97**, 259-271 (2015).
24 Getz, G. S. Thematic review series: the immune system and atherogenesis. Bridging the innate and adaptive immune systems. *Journal of lipid research* **46**, 619-622 (2005).
25 Aspiras, A. C., Rohner, N., Martineau, B., Borowsky, R. L. & Tabin, C. J. Melanocortin 4 receptor mutations contribute to the adaptation of cavefish to nutrient-poor conditions. *Proceedings of the National Academy of Sciences of the United States of America* **112**, 9668-9673 (2015).
26 Xiong, S., Krishnan, J., Peuss, R. & Rohner, N. Early adipogenesis contributes to excess fat accumulation in cave populations of Astyanax mexicanus. *Developmental biology* **441**, 297-304 (2018).
27 Kalbe, M., Wegner, K. M. & Reusch, T. B. H. Dispersion patterns of parasites in 0+ year three-spined sticklebacks: a cross population comparison. *Journal of Fish Biology* **60**, 1529-1542 (2002).
28 Wiens, G. D. & Vallejo, R. L. Temporal and pathogen-load dependent changes in rainbow trout (Oncorhynchus mykiss) immune response traits following challenge with biotype 2 Yersinia ruckeri. *Fish & shellfish immunology* **29**, 639-647 (2010).
29 Prusall, E. R. & Rolff, J. in *Ecoimmunology* Vol. 1st edition 530-548 (Oxford University Press, 2011).
30 Traver, D. *et al.* Transplantation and in vivo imaging of multilineage engraftment in zebrafish bloodless mutants. *Nature immunology* **4**, 1238-1246 (2003).
31 Lugo-Villarino, G. *et al.* Identification of dendritic antigen-presenting cells in the zebrafish. *Proceedings of the National Academy of Sciences of the United States of America* **107**, 15850-15855 (2010).
32 Wittamer, V., Bertrand, J. Y., Gutschow, P. W. & Traver, D. Characterization of the mononuclear phagocyte system in zebrafish. *Blood* **117**, 7126-7135 (2011).

33 Stockdale, W. T. *et al.* Heart Regeneration in the Mexican Cavefish. *Cell reports* **25**, 1997-2007 e1997 (2018).
34 Ogryzko, N. V., Renshaw, S. A. & Wilson, H. L. The IL-1 family in fish: swimming through the muddy waters of inflammasome evolution. *Developmental and comparative immunology* **46**, 53-62 (2014).
35 Sunyer, J. O. Evolutionary and Functional Relationships of B Cells from Fish and Mammals: Insights into their Novel Roles in Phagocytosis and Presentation of Particulate Antigen. *Infectious Disorders - Drug Targets* **12**, 200-212 (2012).
36 Bolnick, D. I., Shim, K. C., Schmerer, M. & Brock, C. D. Population-Specific Covariation between Immune Function and Color of Nesting Male Threespine Stickleback. *PloS one* **10**, e0126000 (2015).
37 Peuß, R. *et al.* Label-independent flow cytometry and unsupervised neural network method for de novo clustering of cell populations. *bioRxiv*, 603035 (2019).
38 van der Meer, W., Scott, C. S. & de Keijzer, M. H. Automated flagging influences the inconsistency and bias of band cell and atypical lymphocyte morphological differentials. *Clin Chem Lab Med* **42**, 371-377 (2004).
39 Wan, F. *et al.* Characterization of gammadelta T Cells from Zebrafish Provides Insights into Their Important Role in Adaptive Humoral Immunity. *Frontiers in immunology* **7**, 675 (2016).
40 Fan, X. & Rudensky, A. Y. Hallmarks of Tissue-Resident Lymphocytes. *Cell* **164**, 1198-1211 (2016).
41 Rossi, D. J. *et al.* Cell intrinsic alterations underlie hematopoietic stem cell aging. *Proceedings of the National Academy of Sciences of the United States of America* **102**, 9194-9199 (2005).
42 Bolli, N. *et al.* Expression of the cytoplasmic NPM1 mutant (NPMc+) causes the expansion of hematopoietic cells in zebrafish. *Blood* **115**, 3329-3340 (2010).
43 Stachura, D. L. *et al.* Clonal analysis of hematopoietic progenitor cells in the zebrafish. *Blood* **118**, 1274-1282 (2011).
44 Reavie, L. *et al.* Regulation of hematopoietic stem cell differentiation by a single ubiquitin ligase-substrate complex. *Nature immunology* **11**, 207-215 (2010).
45 Cabezas-Wallscheid, N. *et al.* Identification of regulatory networks in HSCs and their immediate progeny via integrated proteome, transcriptome, and DNA methylome analysis. *Cell stem cell* **15**, 507-522 (2014).
46 Cheng, J. *et al.* Hematopoietic defects in mice lacking the sialomucin CD34. *Blood* **87**, 479-490 (1996).
47 Anjos-Afonso, F. *et al.* CD34(-) cells at the apex of the human hematopoietic stem cell hierarchy have distinctive cellular and molecular signatures. *Cell stem cell* **13**, 161-174 (2013).
48 Amin, R. H. & Schlissel, M. S. Foxo1 directly regulates the transcription of recombination-activating genes during B cell development. *Nature immunology* **9**, 613-622 (2008).
49 Han, S., Zheng, B., Schatz, D. G., Spanopoulou, E. & Kelsoe, G. Neoteny in lymphocytes: Rag1 and Rag2 expression in germinal center B cells. *Science* **274**, 2094-2097 (1996).
50 Fänge, R. & Nilsson, S. The fish spleen: structure and function. *Experientia* **41**, 152-158 (1985).
51 Naito, Y. *et al.* Germinal center marker GL7 probes activation-dependent repression of N-glycolylneuraminic acid, a sialic acid species involved in the negative modulation of B-cell activation. *Molecular and cellular biology* **27**, 3008-3022 (2007).
52 Liu, T., Zhang, L., Joo, D. & Sun, S. C. NF-kappaB signaling in inflammation. *Signal transduction and targeted therapy* **2** (2017).
53 Secombes, C. J., Wang, T. & Bird, S. The interleukins of fish. *Developmental and comparative immunology* **35**, 1336-1345 (2011).

54 Steinel, N. C. & Bolnick, D. I. Melanomacrophage Centers As a Histological Indicator of Immune Function in Fish and Other Poikilotherms. *Frontiers in immunology* **8**, 827 (2017).
55 Weisberg, S. P. *et al.* Obesity is associated with macrophage accumulation in adipose tissue. *J Clin Invest* **112**, 1796-1808 (2003).
56 Heidt, T. *et al.* Chronic variable stress activates hematopoietic stem cells. *Nature medicine* **20**, 754-758 (2014).
57 Christ, A. *et al.* Western Diet Triggers NLRP3-Dependent Innate Immune Reprogramming. *Cell* **172**, 162-175 e114 (2018).
58 McAlpine, C. S. *et al.* Sleep modulates haematopoiesis and protects against atherosclerosis. *Nature* (2019).
59 Peuss, R., Eggert, H., Armitage, S. A. & Kurtz, J. Downregulation of the evolutionary capacitor Hsp90 is mediated by social cues. *Proceedings. Biological sciences* **282** (2015).
60 Pfaffl, M. W., Horgan, G. W. & Dempfle, L. Relative expression software tool (REST(C)) for group-wise comparison and statistical analysis of relative expression results in real-time PCR. *Nucleic Acids Research* **30**, 36e-36 (2002).
61 Zhang, Y. A. *et al.* IgT, a primitive immunoglobulin class specialized in mucosal immunity. *Nature immunology* **11**, 827-835 (2010).
62 Rowe, R. G., Mandelbaum, J., Zon, L. I. & Daley, G. Q. Engineering Hematopoietic Stem Cells: Lessons from Development. *Cell stem cell* **18**, 707-720 (2016).
63 Stachura, D. L. *et al.* The zebrafish granulocyte colony-stimulating factors (Gcsfs): 2 paralogous cytokines and their roles in hematopoietic development and maintenance. *Blood* **122**, 3918-3928 (2013).
64 de Jong, J. L. & Zon, L. I. Use of the zebrafish system to study primitive and definitive hematopoiesis. *Annual review of genetics* **39**, 481-501 (2005).
65 Athanasiadis, E. I. *et al.* Single-cell RNA-sequencing uncovers transcriptional states and fate decisions in haematopoiesis. *Nature communications* **8**, 2045 (2017).
66 Zeng, A. *et al.* Prospectively Isolated Tetraspanin(+) Neoblasts Are Adult Pluripotent Stem Cells Underlying Planaria Regeneration. *Cell* **173**, 1593-1608 e1520 (2018).
67 Schindelin, J. *et al.* Fiji: an open-source platform for biological-image analysis. *Nature methods* **9**, 676-682 (2012).
68 Sun, K. *et al.* Endotrophin triggers adipose tissue fibrosis and metabolic dysfunction. *Nature communications* **5**, 3485 (2014).
69 R: A language and environment for statistical computing (R Foundation for Statistical Computing, Vienna, Austria, 2014).
70 Benjamini, Y. & Hochberg, Y. Controlling the False Discovery Rate: A Practical and Powerful Approach to Multiple Testing. *Journal of the Royal Statistical Society: Series B (Methodological)* **57**, 289-300 (1995).
71 Samusik, N., Good, Z., Spitzer, M. H., Davis, K. L. & Nolan, G. P. Automated mapping of phenotype space with single-cell data. *Nature methods* **13**, 493-496 (2016).

Supplemental Figures

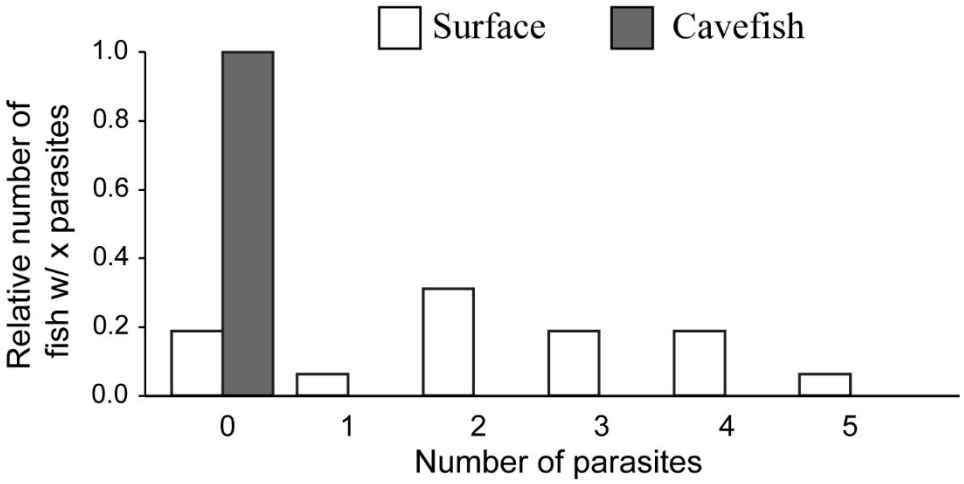

Figure S1: Numbers of different macroparasites found in wild surface (Río Choy) or cavefish (Pachón).

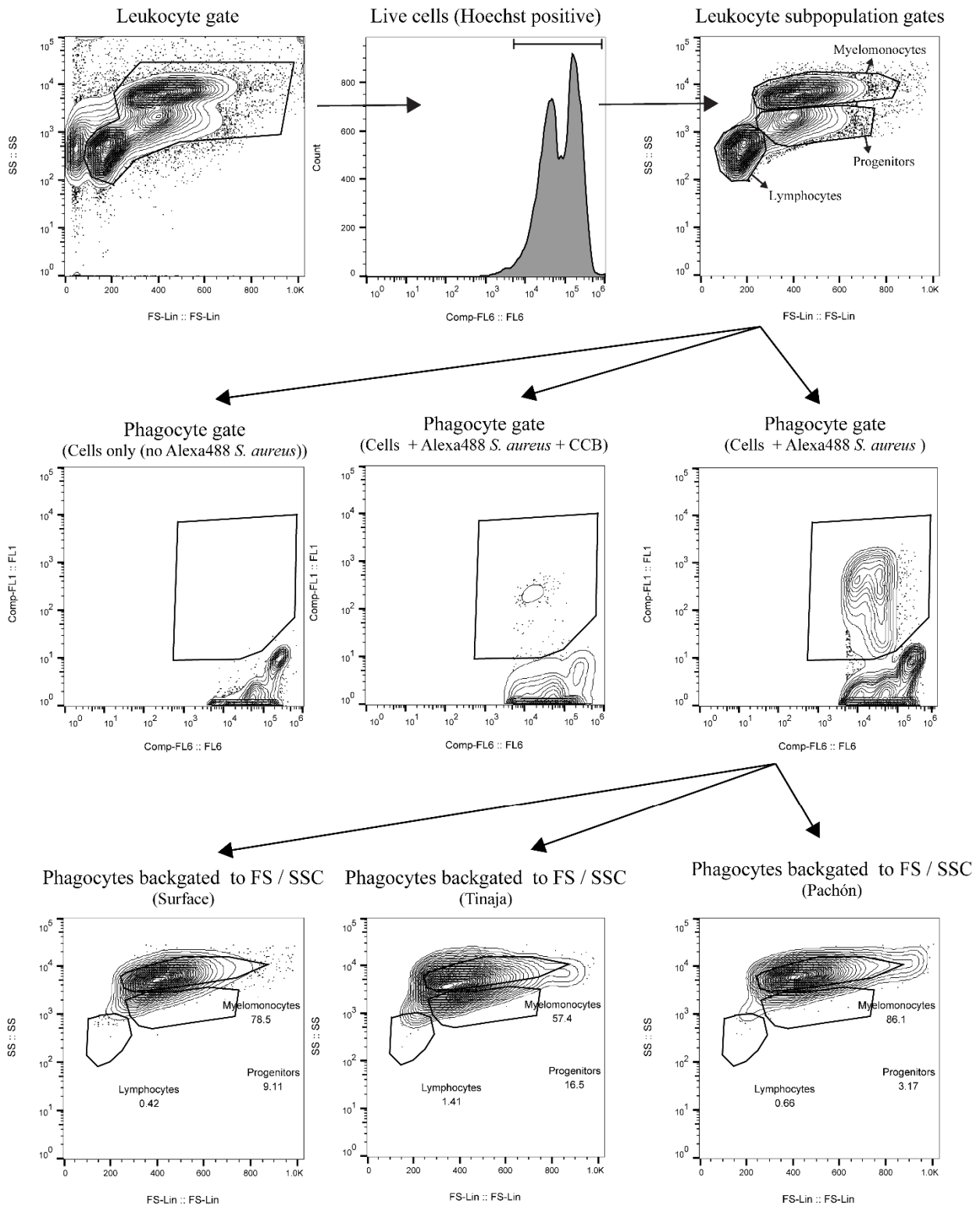

Figure S2: Gating strategy to identify phagocytes in head kidney cell suspension from Astyanax mexicanus using Alexa-488 Staphylococcus aureus and cytochalasin-B (CCB) as a control for active phagocytosis.

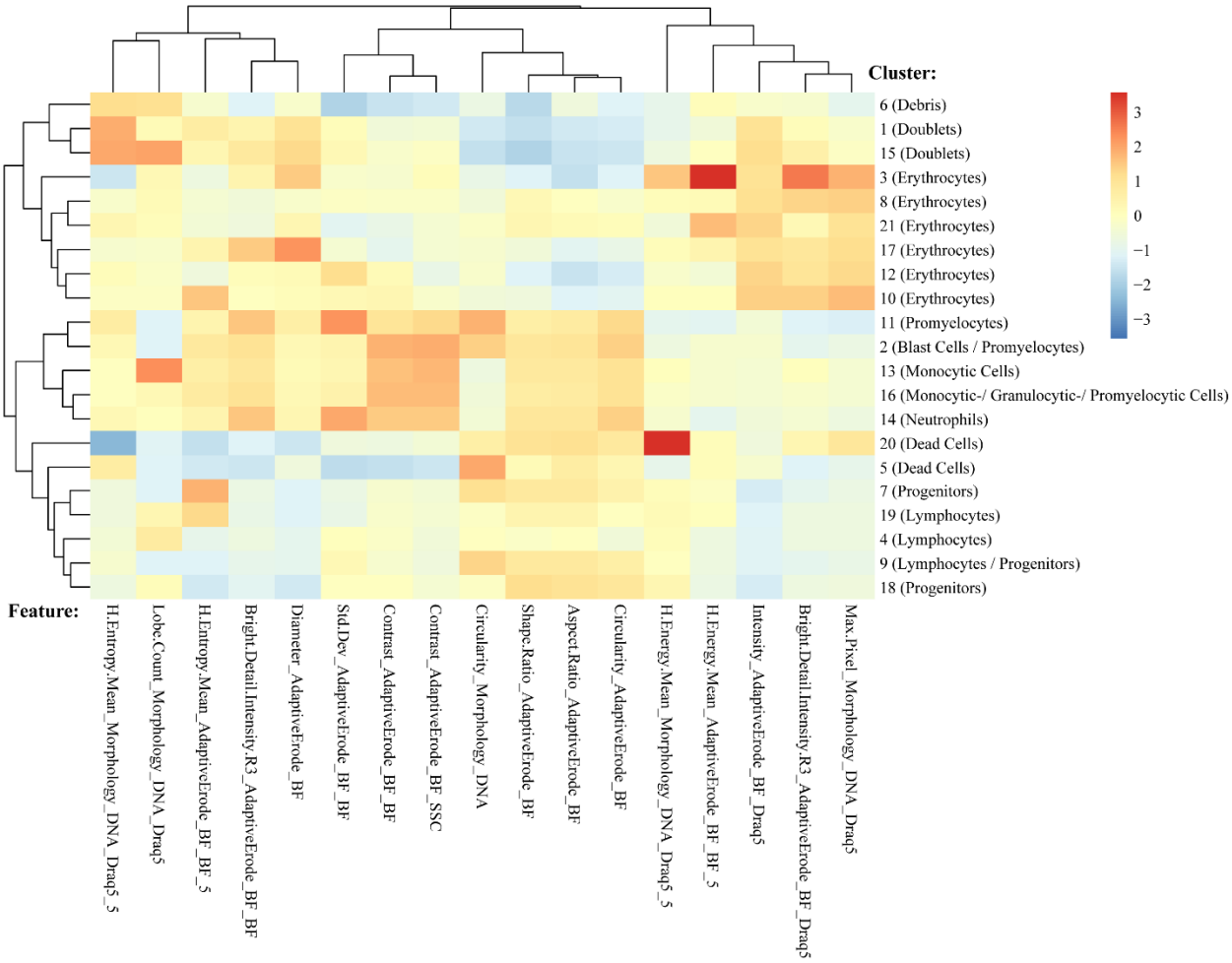

Figure S3: Spearmen Correlation of overall mean feature intensities used for clustering and single cluster after X-shift based clustering using head kidney cells from surface fish and cavefish. See Table S3 for details of features.

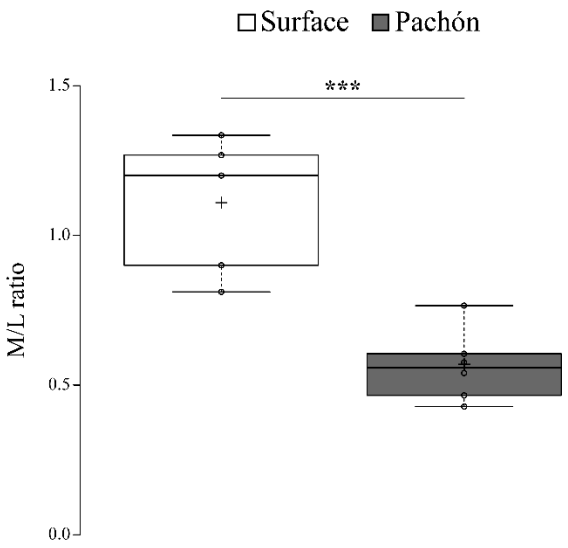

Figure S4: Myelomonocyte/ lymphocyte ratio based on Image3C analysis. Differences between surface fish (Río Choy) and cavefish (Pachón) were tested using a one-way Anova. Significances are indicated as *** for $p \leq 0.001$.

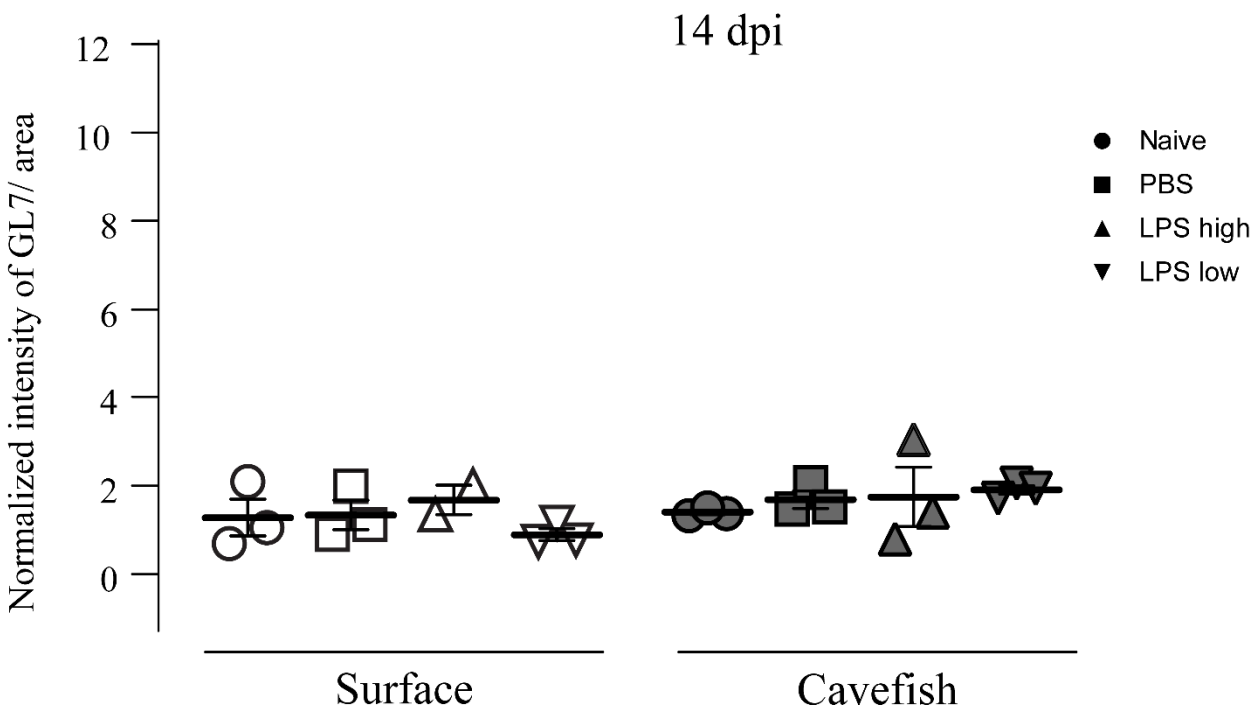

Figure S5: Antibody staining (rat anti-GL7 Alexa Fluor® 647 (BD Pharmingen™) of activated B- and T-cells within germinal center of the spleen 14 days post injection (dpi) of either PBS (20µL/ g fish bodyweight), a high dose of LPS (LPS high; 20µg in 20µL/ g fish bodyweight) or a low dose of LPS (LPS low; 5µg in 20µL/ g fish bodyweight) or left naïve (not injected) as a control group.

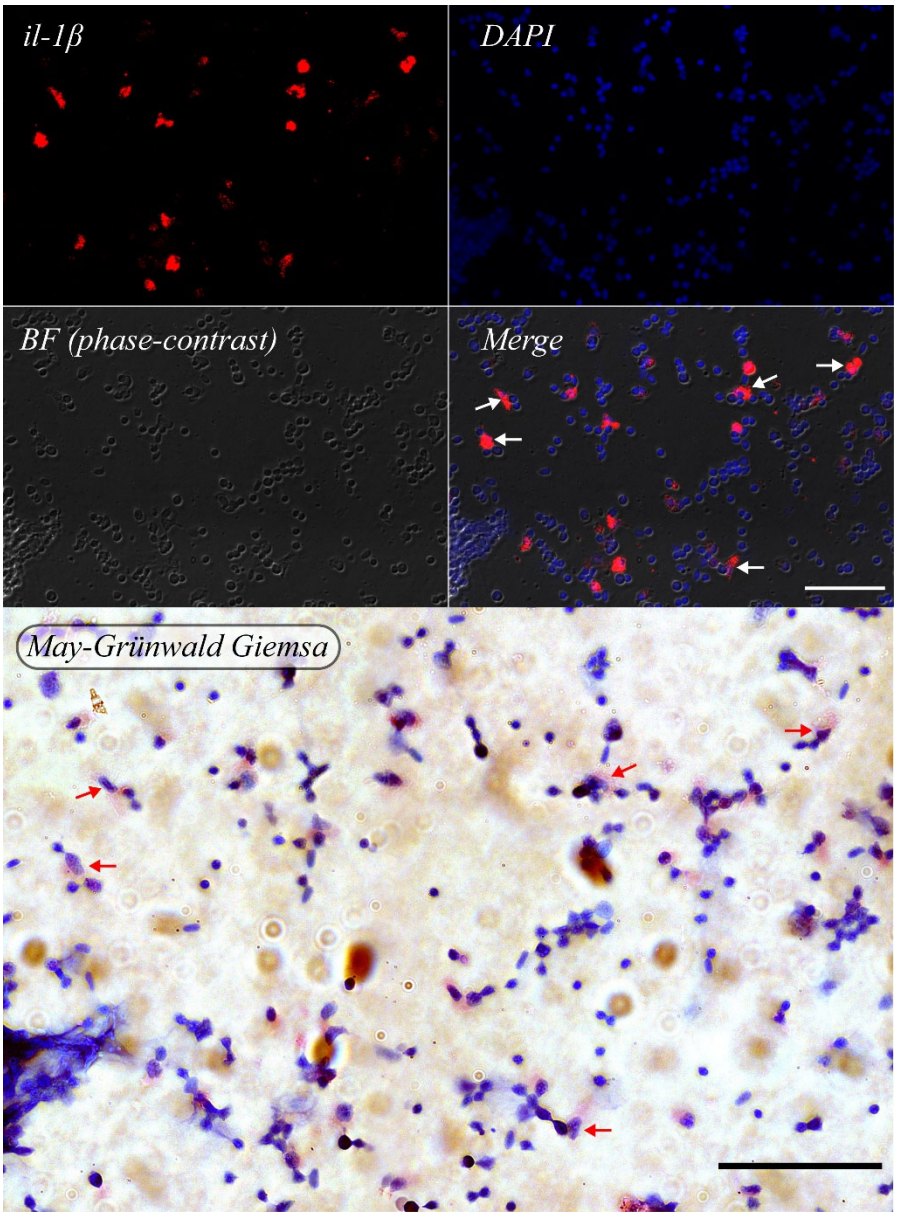

Figure S6: RNAscope analysis on dissociated head kidney cells from surface fish 3hpi with LPS (20µg in 20µL/g bodyweight). Dissociated cells were transferred on Microscope slide and stained as described in Supplemental Methods. After RNAscope imagining using 700/75 nm and 455/50 nm filter for the far red channel (*il-1β*) and DAPI channel, respectively, cover slip was removed and cells were stained after May-Grünwald Giemsa. Exact position of slide was imaged with 63 X Oil objective as before. Cells expressing *il-1β* are marked with white arrow in '*Merge*' image and the same cells are marked with a red arrow in '*May-Grünwald Giemsa*' image.

Supplemental Tables

Table S1: Primer-sequences with respective efficiencies (E) for RT-qPCR.

Gene Symbol	Name	Gene Accession Number	E / Fragment length bp	5' – 3' primer sequence	Primer origin
Il-1β	*Interleukin 1 beta*	XM_022680751	1.99 / 78	F: AGGAAACCAGAGTCAGAGCG R: GGCTGACCCTTTGTGGAGTT	This study
tnf-α	*Tumor necrosis factor alpha*	XM_015602024	1.97 / 154	F: TCTGGCTATAGCTGTGTGCG R: TGGGTTGTAGTGACCTGACA	This study
Il-6	*Interleukin 6*	XM_022668071	1.99 / 116	F: CTGCGGGATGAGCAGTTTCA R: TTGTGTCGGCACCTGTCTTC	This study
g-csf	*Granulocyte colony froming factor*	XM_007255159	1.95 / 138	F: TGCAGAATCCTGCCTTCGAG R: GTTTGCCTGAGTCATTGCCG	This study
rpl32	*Ribosomal protein L32*	XM_007251493	1.99 / 144	F: CGCTTTAAGGGACAGATGCT R: GTAGCTCTTGTTGCTCATCA	This study
rpl13a	*Ribosomal protein L13a*	XM_007244599	1.99 / 147	F: TCTGGAGGACTGTAAGAGGTATGC R: AGACGCACAATCTTGAGAGCAG	Beale, Guibal [1]

1. Beale, A. *et al.* Circadian rhythms in Mexican blind cavefish Astyanax mexicanus in the lab and in the field. *Nature communications* **4**, 2769 (2013).

Table S2: Overview of features extracted for morphological identification of *A. mexicanus* head kidney cells.

Feature ID	Feature_ImageMask_Channel	Feature description
1	Area_AdaptiveErode_BF	Cell size
2	Area_Intensity_SSC	Areas of SSC signal above background
3	Area_Morphology_DNA	Area of DNA signal (nuclear staining)
4	Aspect.Ratio_AdaptiveErode_BF	Aspect ratio of total cell area
5	Bright.Detail.Intensity.R3_AdaptiveErode_BF_BF	Intensity of brightest staining areas
6	Bright.Detail.Intensity.R3_AdaptiveErode_BF_Draq5	Intensity of brightest staining areas
7	Bright.Detail.Intensity.R3_AdaptiveErode_BF_SSC	Intensity of brightest signal areas
8	Circularity_AdaptiveErode_BF	Circularity of whole cell shape
9	Circularity_Morphology_DNA	Circularity of nucleus
10	Contrast_AdaptiveErode_BF_BF	Detects large changes in pixel values - can be measure of granularity of signal
11	Contrast_AdaptiveErode_BF_SSC	Detects large changes in pixel values - can be measure of granularity of signal
12	Diameter_AdaptiveErode_BF	Diameter of whole cell shape
13	Diameter_Morphology_DNA	Diameter of nucleus
14	H.Energy.Mean_AdaptiveErode_BF_BF_5	Measure of intensity concentration - texture feature
15	H.Energy.Mean_Morphology_DNA_Draq5_5	Measure of intensity concentration - texture feature
16	H.Entropy.Mean_AdaptiveErode_BF_BF_5	Measure of intensity concentration and randomness of signal - texture feature
17	H.Entropy.Mean_Morphology_DNA_Draq5_5	Measure of intensity concentration and randomness of signal - texture feature
18	Intensity_AdaptiveErode_BF_Draq5	Integrated intensity of signal within whole cell mask
19	Intensity_AdaptiveErode_BF_SSC	Integrated intensity of signal within whole cell mask
20	Lobe.Count_Morphology_DNA_Draq5	Number of lobes of nucleus
21	Max.Pixel_Intensity_Ch6_SSC	maximum pixel intensity of stated channel within a whole cell mask
22	Max.Pixel_Morphology_DNA_Draq5	maximum pixel intensity of stated channel within a whole cell mask
23	Mean.Pixel_Morphology_DNA_Draq5	mean pixel intensity of stated channel within a whole cell mask
24	Shape.Ratio_AdaptiveErode_BF	minimum thickness divided by length - measure of cell shape characterisic
25	Std.Dev_AdaptiveErode_BF_BF	standard deviation of BF signal - measure of granularity and variance in BF